

https://dspace.org/

Thermodynamics of Complexation: Variant R15L hGST A1-1 binding to ANS and GSO3

Dobreva, Marina Alexandrova

2006-10-31T09:29:16Z
http://hdl.handle.net/10539/1519

Downloaded from a DSpace repository. https://dspace.org/

Thermodynamics of Complexation: Variant R15L hGST A1-1 binding to ANS and GSO_3^-

Marina Alexandrova Dobreva

A dissertation submitted to the Faculty of Science, University of the Witwatersrand, Johannesburg, in fulfillment of the requirements for the degree of Master of Science.

Johannesburg, September 2005

Declaration

I declare that this dissertation is my own, unaided work. It is being submitted for the degree of Master of Science in the University of the Witwatersrand, Johannesburg. It has not been submitted before for any degree or examination at any other University.

M. A. Dobreva

day of 2005.

This work is dedicated to life, the greatest teacher of all:
"Non scholae, sed vitae discimus"
(Roman sententia)

If

If you can keep your head when all about you
Are losing theirs and blaming it on you;
If you can trust yourself when all men doubt you,
But make allowance for their doubting too;
If you can wait and not be tired by waiting,
Or being lied about, don't deal in lies,
Or being hated, don't give way to hating,
And yet don't look too good, nor talk too wise:

If you can dream -- and not make dreams your master;
If you can think -- and not make thoughts your aim;
If you can meet with Triumph and Disaster
And treat those two imposters just the same;
If you can bear to hear the truth you've spoken
Twisted by knaves to make a trap for fools,
Or watch the things you gave your life to, broken,
And stoop and build 'em up with worn-out tools;

If you can make one heap of all your winnings
And risk it on one turn of pitch-and-toss,
And lose, and start again at your beginnings
And never breathe a word about your loss;
If you can force your heart and nerve and sinew
To serve your turn long after they are gone,
And so hold on when there is nothing in you
Except the Will which says to them: "Hold on!"

If you can talk with crowds and keep your virtue,
Or walk with kings -- nor lose the common touch,
If neither foes nor loving friends can hurt you,
If all men count with you, but none too much;
If you can fill the unforgiving minute
With sixty seconds' worth of distance run --
Yours is the Earth and everything that's in it,
And -- which is more -- you'll be a Man, my son!

Rudyard Kipling

Abstract

Positive charges play an important role in the active site of a variety of proteins including alpha class GST. The presence of Arg15 at the subunit interface between the H- and G-site of hGST A1-1 was shown to be important for the catalytic function of the enzyme, thus providing an electrostatic potential in the G-site. This electrostatic potential favours ionisation and activation of GSH bound to hGST A1-1. Although much is known regarding the catalytic function of GSTs, little is known of the effect of Arg15 on the binding of glutathione conjugates and nonsubstrate ligands. Others (Matulis and Lovrien, 1998) have pointed out that binding of the nonsubstrate ligand ANS is accomplished via ion pair formation with a charged residue such as Arg. Therefore, in order to evaluate the importance of the positive charge provided by the side chain of Arg15 in the active site of hGST A1-1 protein engineering techniques were employed to generate an R15L variant. The variant does not display a detectable difference in the secondary or tertiary structural content relative to the wild type hGST A1-1 protein. The catalytic activity of the R15L variant is, however, substantially reduced indicating local tertiary structural changes at and possibly near the active site. In the presence of ANS the fluorescence spectra of the variant R15L protein had a significantly lower intensity relative to wild type protein indicating either increased exposure of hydrophobic surface area at the H-site and/or reduced number of ANS molecules bound (i.e., reduced affinity). Although ANS is displaced by GSO_3^- in the wild type protein, no such displacement is observed for the R15L variant protein. Isothermal titration calorimetry experiments for GSO_3^- and ANS binding to R15L indicated that the variant protein binds GSO_3^- more tightly (higher affinity) than ANS (lower affinity). The above information, taken together, argues in favour of both molecules (ANS and GSO_3^-) occupying the active site of R15L simultaneously. Despite the fact that there is no experimental crystal structure of hGST A1-1 complexed with either of the ligands, the placement of ANS was argued (Dirr *et al.*, 2005) to be at the H-site and of GSO_3^- at the G-site of the protein. The binding of ANS is both enthalpically and entropically favourable over the temperature range investigated (5 to 25°C) indicating expulsion of water molecules from the active site as well as the lack of a localised C-terminal α9 helix. The hydrophobic character of both the ligand and the

site which accommodates it (H-site) contribute favourably towards the reaction enthalpy. ANS is conformationaly more constrained than GSO_3^- when found free in solution, thus exhibiting more favourable conformational entropy change upon binding to R15L variant. The binding of GSO_3^- is enthalpically favourable but entropically opposed. The expulsion of water molecules from the G-site, which accommodates GSO_3^-, is insufficient to compensate for the loss of conformational entropy of both the ligand and C-terminal α9 helix, which becomes localised upon binding. However, favourable enthalpic contributions arise from the formation of hydrogen bonds, salt links and van der Waals contacts between the R15L variant and the ligand and the C-terminal α9 helix. Arg15 forms a salt link with Glu104 of the neighbouring domain and therefore provided an ideal opportunity to evaluate the role of Arg15 and its impact on interdomain stability. Conformational stability and unfolding studies of the R15L variant, monitored via fluorescence, indicated that the variant deviates from the model of a two-state transition. There are no stable thermodynamic intermediate(s) observed, but the increase in the *m*-value is an indicator of a transition state which is more stable against urea relative to the wild type protein. Kinetically (Wallace *et al.*, 1998b), the wild type hGST A1-1 follows a three-state unfolding transition where the kinetic intermediate is defined as having undergone conformational changes at the domain-domain interface and the C-terminal region. The substitution of Arg15 with Leu may have impacted on the packing of the native form of the variant R15L relative to the wild type GST A1-1, thus rendering the R15L protein more stable against urea. Arg15, therefore, may have an important role at the interdomain interface of GSTs.

Acknowledgments

I would like to thank the following people:

My Mother for her never-ending comfort in my life.

My Father for his jokes in times when laughter was most needed.

Professor Heini Dirr for his guidance, encouragement and support over the course of my studies. Thank you for the opportunity and privilege of working in your lab. Words can hardly express my infinite gratitude.

Dr. Yasien Sayed for his assistance and support throughout my studies. Thank you for the words of encouragement and motivation when such were needed.

Carla Alves for just being there when I needed a friend the most.

The members of the Protein Structure-Function Research Programme, University of the Witwatersrand for all their assistance.

The University of the Witwatersrand and the South African National Research Foundation for financial support.

Table of contents:

Declaration ii

Abstract iv

Acknowledgments vi

Abbreviations x

List of Figures: xii

List of Tables: xiv

Chapter 1 Introduction 1

1.1 Molecular recognition and thermodynamics 1

1.1.1 Thermodynamics of protein-ligand interactions 1

1.1.2 Practical considerations of ITC 6

1.1.2.1 ΔG, K_a and the *c*-value 6

1.1.2.2 Control experiments 7

1.1.2.3 Protonation effects 8

1.1.3 Informational content of ITC data 9

1.1.3.1 Binding free energy 9

1.1.3.2 Binding enthalpy 10

1.1.3.3 Binding entropy 11

1.1.3.4 Heat capacity change 11

1.1.3.5 Enthalpy-entropy compensation 12

1.2 Glutathione *S*-transferase 12

1.2.1 Class Alpha glutathione transferase 13

1.2.2 Unfolding and stability of hGST A1-1 16

1.2.3 Active site 17

1.2.3.1 Glutathione binding site 17

1.2.3.2 Hydrophobic substrate binding site 19

1.2.3.3 Catalytic mechanism 20

1.2.4 Non-substrate ligand binding site ... 22
1.2.5 R15L hGST A1-1 variant ... 22
Objectives ... 25

Chapter 2 Experimental procedures ... 27

2.1 Materials ... 27
2.2 Construction of the R15L variant by site-directed mutagenesis ... 27
2.2.1 Oligonucleotide primer design ... 27
2.2.2 Site-directed mutagenesis ... 27
2.2.3 Sequencing of the mutant plasmid DNA ... 28
2.3 Overexpression and purification of wild type and R15L ... 28
2.3.1 Induction studies ... 29
2.3.2 Overexpression and purification ... 29
2.3.3 Protein concentration determination ... 30
2.3.4 Sodium dodecyl sulphate polyacrylamide gel electrophoresis ... 31
2.4 Steady-state kinetics ... 31
2.4.1 Enzyme assay ... 31
2.4.2 BSP inhibition ... 32
2.5 Spectroscopic studies ... 32
2.5.1 Spectra determination ... 32
2.5.2 Unfolding studies ... 32
2.5.2.1 Reversibility of unfolding ... 32
2.5.2.2 Urea-induced equilibrium unfolding ... 33
2.5.2.3 Two-state fitting model for the unfolding transitions ($N_2 \leftrightarrow 2U$) ... 33
2.5.3 Determination of dissociation constants ... 35
2.6 Isothermal titration calorimetry ... 35
2.6.1 ANS and GSO_3^- binding to R15L ... 35
2.6.2 Temperature dependence of thermodynamic parameters ... 36

Chapter 3 Results ... 37

3.1 Generation, expression, purification and characterisation of R15L hGST A1-1 variant 37
3.2 Conformational stability and unfolding of R15L 43
3.3 Steady state enzyme kinetics 46
3.3.1 CDNB conjugating activity of R15L 46
3.3.2 The effect of BSP on CDNB conjugating activity of R15L 46
3.4 Displacement studies 49
3.4.1 Spectral properties of hGST A1-1 and R15L bound ANS 49
3.4.2 Glutathione sulphonate displacement of ANS 52
3.5 Isothermal titration calorimetry 52

Chapter 4 Discussion and Conclusion 62

4.1 Conformational stability 62
4.2 Isothermal titration calorimetry 64
4.3 Conclusion 73

Chapter 5 References: 75

Abbreviations

AFB_1	aflatoxin B_1
ΔASA	change in solvent accessible surface area
$\Delta G(H_2O)$	change in Gibbs free energy of unfolding in the absence of denaturant
ε_{280}	molar extinction coefficient at 280 nm
$[\theta]$	mean residue ellipticity
A_{280}	absorbance at 280 nm
ANS	8-anilino-1-napthalene sulphonate
CD	circular dichroism
ΔC_p	change in heat capacity
CDNB	1-chloro-2,4-dinitrobenzene
CNB	1-chloro-4-nitrobenzene
C_m	urea-induced midpoint of unfolding
DSC	differential scanning calorimetry
EDTA	ethylenediaminetetra-acetic acid
ΔG	change in Gibbs free energy
GSH	reduced glutathione
G-site	glutathione binding site
GST	glutathione *S*-transferase
ΔH	change in enthalpy
hGST A1-1	human class Alpha glutathione transferase with two type 1 monomers
hGST P1-1	human class Pi glutathione transferase with two type 1 monomers
HMBA	4-(hydroxymethyl)-benzoic acid
HNBA	2-hydroxy-5-nitrobenzyl alcohol
H-site	hydrophobic electrophilic substrate binding site

IPTG	isopropyl-β-D-thiogalactoside
K_a	association constant (affinity constant)
K_d	dissociation constant
L	ligand
LB	Luria-Bertani
M	macromolecule (protein)
N	stoichiometry of the reacting species
m-value	susceptibility of the protein to denaturant
N_2	native folded dimer
NaCl	sodium chloride
OD_{600}	optical density at 600 nm
PBA	4-propylbenzoic acid
PDB	Protein Data Bank
R	universal gas constant
rGST A1-1	rat class Alpha glutathione transferase with two type 1 monomers
ΔS	change in entropy
SDS/PAGE	sodium dodecyl sulphate-polyacrylamide gel electrophoresis
T	temperature in degrees kelvin
TSA	4-toluenesulphonic acid
U	unfolded monomer
wt	wild type protein

The IUPAC-IUBMB three and one letter codes for amino acids are used.

List of Figures:

Figure 1. Isothermal titration calorimeter. 3
Figure 2. A representative calorimetric titration profile for binding of GSO_3^- to Δ Phe222 hGST A1-1. 4
Figure 3 A ribbon representation of homodimeric hGST A1-1 as viewed down the two-fold axis (pdb code: 1guh; (Sinning *et al.*, 1993)). 14
Figure 4. Ribbon representation of the crystal structure of hGST A1-1(pdb code 1k3l; (Le Trong *et al.*, 2002)). 15
Figure 5 Schemiatic representation of bound *S*-benzyl-glutathione in the G-site of hGST A1-1.. 18
Figure 6. A schematic representation of GST catalysed conjugation of glutathione to CDNB. 21
Figure 7. Generation of R15L. 38
Figure 8. 15% SDS-PAGE separation of *Escherichia coli* BL21 (DE3) proteins from induction studies done with over-expressed R15L variant. 39
Figure 9. 15% SDS-PAGE of purified R15L and a calibration curve. 41
Figure 10. Far-UV circular dichroism spectra characterisation of the wild type hGST A1-1 (---) and the variant R15L (---) proteins in 20 mM sodium phosphate buffer, pH 6.5, containing 1mM EDTA and 0.02% sodium azide. 42
Figure 11. Urea-induced equilibrium unfolding curves for R15L. 44
Figure 12. Determination of the specific activity of the (A) wild type and (B) R15L proteins. 47
Figure 13. Inhibition of wild type and R15L hGST A1-1 CDNB-conjugating activity by BSP.. 48
Figure 14. Fluorescence spectral characterisation of wild type (blue and black) and R15L (red and green) 50
Figure 15. The structure of the organic anionic dye ANS. 51
Figure 16. The structure of the GST ligand glutathione sulphonate. 53
Figure 17. Displacement of ANS bound to wt hGST A1-1(●) and R15L(■) by GSO_3^-... 54

Figure 18. A calorimetric profile for the titration of R15L hGST A1-1 with ANS..... 55
Figure 19 A calorimetric profile for the titration of R15L hGST A1-1 with GSO_3^-. 56
Figure 20. Temperature dependence of the thermodynamic parameters for the binding of ANS in the presence of 100 mM NaCl. 60
Figure 21. Temperature dependence of the thermodynamic parameters for the binding of GSO_3^- in the presence of 100 mM NaCl. 61

List of Tables:

Table 1. Specific activity of hGST A1-1 and eight Arg variants for three substrates…...23

Table 2. IC_{50} values for various inhibitors of hGST A1-1 and Arg variants of the protein……23

Table 3. A comparison of thermodynamic properties of the wild type protein with R15L variant determined from unfolding experiments using fluorescence and circular dichroism as probes……...45

Table 4. Thermodynamic parameters for the binding of ANS to R15L hGST A1-1 at various temperatures…….58

Table 5. Thermodynamic parameters for the binding of GSO_3^- to R15L hGST A1-1 at various temperatures…….59

Table 6. Dissociation constants of wild type hGST A1-1 and variant proteins for ANS and GSO_3^-……..66

Chapter 1
Introduction

1.1 Molecular recognition and thermodynamics

Life is based on interactions. Biological phenomena are dependent on molecular recognition, be it inter- or intra-molecular recognition. Protein folding, for example, is based on intramolecular interactions, whereas protein-ligand binding relies on intermolecular recognition (Jelesarov and Bosshard, 1999).

1.1.1 Thermodynamics of protein-ligand interactions

Various parameters are used to describe protein-ligand interactions including affinity constant (K_a), stoichiometry (N), Gibbs free energy (ΔG), enthalpy (ΔH) and entropy (ΔS). All equations linking these terms begin with a simple stoichiometric relationship according to the law of mass action:

$$nL+M \leftrightarrow L_nM \qquad (1)$$

where L is a ligand, M is a protein and n is the number of molecules.

The K_a for this reaction is $[L_nM]/[L]^n[M]$ and the relationship between the affinity constant and the dissociation constant is inversely proportional, i.e., $K_d=1/K_a$. Due to convenience of expression, the dissociation constant, K_d (M) is the most widely used term when investigating thermodynamics.

The K_a and K_d relate to the change in Gibbs free energy for reaction (1) as follows (Wiseman *et al.*, 1989):

$$\Delta G = -RTln\ K_a \text{ or } \Delta G = +RTln\ K_d \qquad (2)$$

The change in Gibbs free energy is a temperature-dependent variable, which is also described by the following equation (Jelesarov and Bosshard, 1999):

$$\Delta G(T)=\Delta H(T_R) + \int \Delta C_p dT - T\Delta S\ (T_R) - T \int \Delta C_p dlnT \qquad (3)$$

where T_R is a reference temperature and $\int$ is the definite integral in the region [$T-T_R$], and ΔC_p is the change in heat capacity. However, there are systems for which the equation can be simplified. For these, the change in heat capacity is independent of temperature (Jelesarov and Bosshard, 1999):

$$\Delta G^o(T)=\Delta H^o(T_R)-T\Delta S^o(T_R) + \Delta C_p(T - T_R - T\ln T/T_R) \quad (4)$$

Enthalpy and entropy changes on the other hand are always dependent on temperature (Jelesarov and Bosshard, 1999):

$$\Delta C_p=d(\Delta H^o)/dT=T\{d(\Delta S^o)/dT\}. \quad (5)$$

Although ΔH^o and ΔS^o are temperature-dependent as mentioned, ΔG^o is practically independent of temperature due to ΔH^o and ΔS^o compensation (Leavitt and Freire, 2001):

$$\Delta G^\circ = \Delta H^\circ - T\Delta S^\circ \quad (6)$$

There are various ways to obtain thermodynamic parameters but only two techniques, isothermal titration calorimetry (ITC) (Figure 1) and differential scanning calorimetry (DSC), directly measure heat or enthalpy (Jelesarov and Bosshard, 1999).

ITC measures the heat exchange (Figure 1), irrespective of whether the heat is absorbed (endothermic process) or released (exothermic process), during complex formation (Jelesarov and Bosshard, 1999; Leavitt and Freire, 2001). When a protein is titrated with an appropriate ligand and the experiment is at constant temperature, the change in heat is measured in terms of electrical power ($cal.s^{-1}$). This is the electrical power needed to maintain a constant temperature difference between the sample and reference cells. The raw data is plotted as peaks (Figure 2(A)), initially large; however, decreasing with the progression of the titration. This is a consequence of the gradual saturation of the protein binding sites with the respective ligand. At the end of the titration, when all of the protein binding sites are

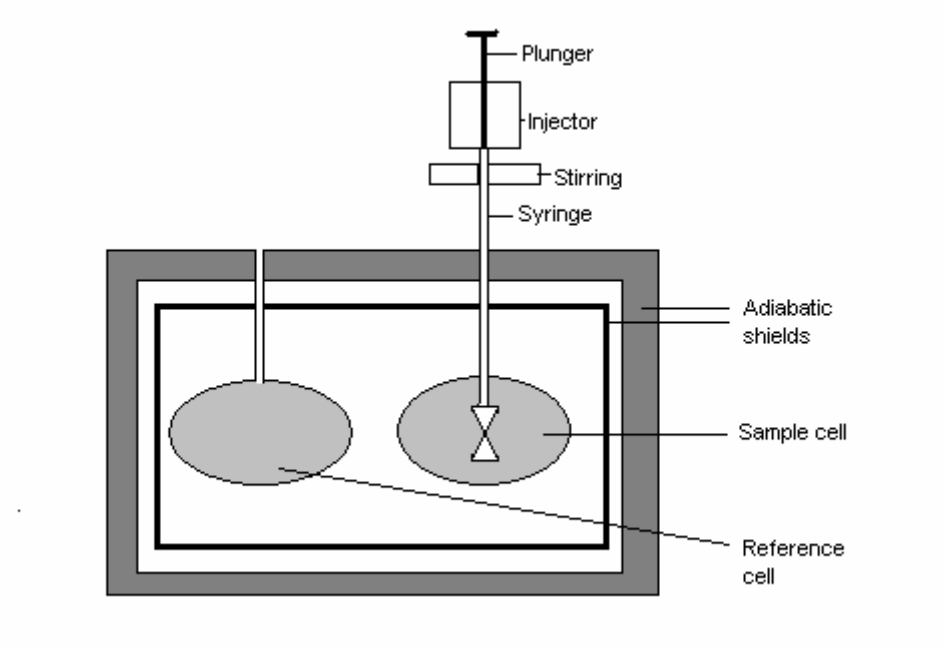


Figure 1. Isothermal titration calorimeter. There are two cells in the calorimeter i.e., the sample and reference cells. The reference cell contains milli-Q water (or buffer) and the sample cell contains the protein solvated in buffer. The ligand is titrated into the sample cell via a syringe. Efficient mixing of the ligand and the protein is accomplished by using the modified syringe end that rotates in place during the ITC experiment. A plunger does precise volume injections of ligand into the sample cell and the titration is controlled via computer There are adiabatic shields surrounding the reference and sample cells so that no heat would escape or enter this isolated system. This keeps the temperature constant for the duration of the experiment. Generated using Microsoft Paint.

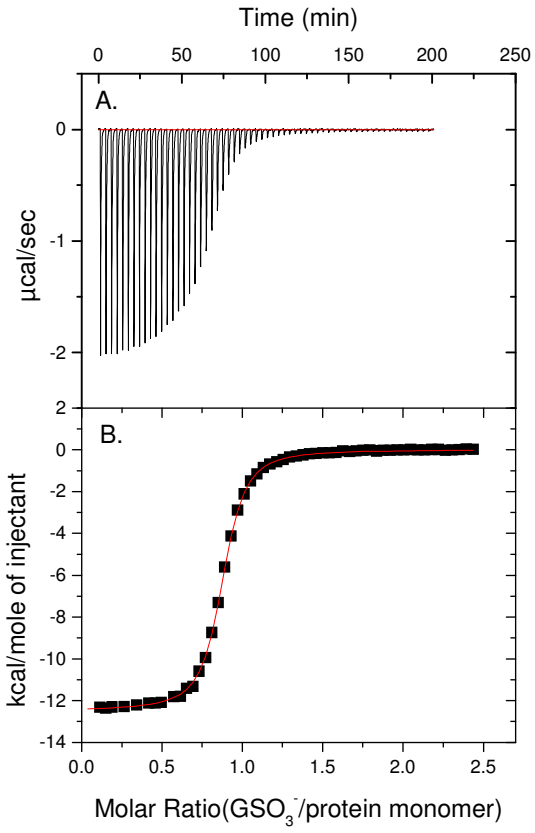


Figure 2. A representative calorimetric titration profile for binding of GSO_3^- to Δ Phe222 hGST A1-1. Panel A: generated exothermic heat with each injection of GSO_3^- into the ITC sample cell containing protein. Panel B: integrated binding isotherm corrected for heats of dilution corresponding to the data in panel A. The solid red line in A and B represent the best fit obtained with ORIGIN 5 software (Dobreva, 2002 unpublished results).

saturated, the small uniform peaks registered are due either to heat of dilution or other nonspecific binding effects. Each peak of the raw data obtained is an expression of the heat released or absorbed upon a single titration step. Integration of the area under each peak with respect to time gives the apparent heat change $\Delta q_{i,app}$ (Jelesarov and Bosshard, 1999):

$$\Delta q_{i,app} = \Delta q_{i} + \Delta q_{i,dil} + \Delta q_{i,ns}$$
$$= \Delta[L_i]_{bound} \times V_{cell} \times \Delta H_{app} \quad (7)$$

where Δq_{i} is the integrated heat of the reaction, $\Delta q_{i,dil}$ is the change in heat effects due to the heat of ligand dilution after saturation, $\Delta q_{i,ns}$ is the change in heat due to nonspecific effects.

$\Delta[L_i]_{bound}$ is the concentration of the bound ligand, V_{cell} is the volume of the calorimetric cell and ΔH_{app} is the apparent molar enthalpy of association.

$\Delta q_{i,dil} + \Delta q_{i,ns}$ are obtained from a blank titration of the buffer with the ligand. The volume of the cell is known (1.457ml for Protein Structure-Function Research Unit VP-ITC) and ΔH_{app} is a constant for a given set of temperature, solvent and pressure conditions. ΔH_{app} and K_a can be calculated from (Jelesarov and Bosshard, 1999):

$$\Delta q_{i} = \Delta q_{i,app} - \Delta q_{i,dil} - \Delta q_{i,ns}$$
$$= n[M]_{tot} \times V_{cell} \times \Delta H_{app} \times \mathcal{R} \quad (8)$$

where $[M]_{tot}$ is the total concentration of M (protein) in the sample sell and $\mathcal{R}$ is the square root of the quadratic equation (Jelesarov and Bosshard, 1999):

$$Y_i^2 - Y_i \times (1 + 1/N\, K_a[M]_{tot} + [L_i]_{tot}/N[M]_{tot}) + N[L_i]_{tot}[M]_{tot} = 0 \quad (9)$$

where Y_i is the degree of saturation ($Y_i = \Delta[L_i]_{bound}/[M]_{tot}$), $[L_i]_{tot}$ is the concentration of the ligand added up to the i^{th} injection and N is the number of binding sites for the ligand L on the protein M. A nonlinear regression of equation (6) would give N, K_a and ΔH_{app} from a plot with typical sigmoidal shape (Figure 2(B)) (Jelesarov and Bosshard, 1999; Leavitt and Freire, 2001; Wiseman *et al.*, 1989).

1.1.2 Practical considerations of ITC

There are three important practical considerations for ITC experiments. The affinity of the protein for the titrated ligand, the control experiments and the proton exchange capacity exhibited between the buffer and the protein. These considerations are discussed below.

1.1.2.1 ΔG, K_a and the c-value

ΔG, which is calculated from the experimentally obtained K_a (see equations (2), (8) and (9)), relates to the spontaneity of the reaction and the reliability of its value is dependent on the concentrations of the interacting species. The reliability of the K_a is also dependent on the concentrations of the interacting species. Therefore, the interacting protein and ligand concentrations need to be in a range where both free ligand and protein-ligand complex are populated. Outside of this range, the concentration of the binding sites on the protein can be either higher or lower than the K_d. Thus, the binding isotherm would either have a rectangular or a shallow sloped sigmoidal shape, rendering K_d determination inaccurate. The rectangular shape of the binding curve with a slope approaching infinity describes a step function, which becomes increasingly insensitive to the changes in K_a. On the other hand, when the shape of the binding curve is very shallow full saturation of the binding sites is difficult to approach (Jelesarov and Bosshard, 1999; Perozzo *et al.*, 2004). The shape of the binding curve, dependant on the binding constant and concentration of the binding sites, is described by a dimensionless number c:

$$c = K_a \, \mathrm{M_t} \, N \qquad (10)$$

where $\mathrm{M_t}$ is a total protein concentration (M).

Most reliable K_a values are given by c-values between 10 and 100, although the upper limit is 1000 and the lower limit is 1 (Wiseman *et al.*, 1989). However, this is not always achievable as some K_a values may be too large or too small to be experimentally determined. This would result in problems with instrument sensitivity or aggregation due to high protein concentration which could interfere with the binding reaction. When the protein-ligand binding is tight, an appropriate pH can be chosen so that the K_a value is

reliable. K_a is often practically independent of temperature changes due to entropy and enthalpy compensations; however, it is dependent on pH fluctuations. Thus, ΔG can be calculated for tight binding at an appropriate pH, provided the pK_a values of the liganded and the ligand-free form of the protein is known and the K_a value is reliable. (Baker and Murphy, 1996; Doyle *et al.*, 1995). Alternatively, displacement reactions of weakly bound ligand by tighter binding ligand can be used if the ligands exhibit a suitable difference in binding enthalpy (Khalifah *et al.*, 1993; Sigurskjold, 2000).

A study done by Turnbull and Daranas (2003) on low affinity systems challenged the canonical lower limit of 1 on the *c*-value and indicated that reliable free energy values can still be obtained under conditions where the *c*-value of the system is in the range of 0.01 and 1. The study also evaluated the reliability of the enthalpy values obtained at this low *c*-value range. However, it was inconclusive with regards to the measured enthalpy as there was a clear trend toward larger negative values as the protein concentration increased (Turnbull and Daranas, 2003). The increase in protein concentration results in elevation of the *c*-value as can be observed from equation (10).

1.1.2.2 Control experiments

The measurement which is done by the isothermal titration calorimeter detects not only the heat which is absorbed or released during a binding reaction but the overall heat effect in the calorimetric cell upon addition of ligand. Thus, the experimental heat effect is comprised of contributions from non-specific heat effects such as diluting of the ligand in the buffer, dilution of the protein sample, temperature differences between the cell and the syringe and mixing of buffers of slightly different composition (Jelesarov and Bosshard, 1999; Perozzo *et al.*, 2004). In order to determine the contributions coming only from the heat of complex formation, the contributions from the heat of non-specific interactions and ligand dilution need to be extracted (see equation (7)). This would necessitate a further three titrations to measure these effects i.e., ligand into buffer, buffer into protein solution and buffer into buffer. However, in practice it was found that the non-specific heat contributions are small and frequently negligible. The heat of ligand dilution, however, may be significant necessitating correction for it as the ligand dilution is typically 10 to 20 times greater than the protein dilution in the course of the reaction.

An alternative to the additional titrations is to design the experiment in such a way that the enzyme binding sites reach saturation before the final injection. Thus, the additional heat effects can be corrected for from the small heats at the end of the titration, and the last several injections can be averaged and subtracted in order to carry out the correction (Jelesarov and Bosshard, 1999; Perozzo *et al.*, 2004; Pierce *et al.*, 1999).

1.1.2.3 Protonation effects

The last point to be considered is the protonation effects, because these contribute towards the measured ΔH_{app}. Protonation effects, when protons exchange with the buffer, will be included in the global ΔH_{app} (Jelesarov and Bosshard, 1999):

$$\Delta H_{app} = \Delta H_{bind} + n_{H+} \times \Delta H_{buffer\ ionisation} \quad (11)$$

where n_{H+} are the number of protons exchanged during the reaction, $\Delta H_{buffer\ ionisation}$ is the ionisation enthalpy of the buffer and ΔH_{bind} is the binding enthalpy. ΔH_{bind} can be described further by the following equation (Jelesarov and Bosshard, 1999):

$$\Delta H_{bind} = \Delta H'_{bind} + n_{H+} \Delta H_{H+} \quad (12)$$

where $\Delta H'_{bind}$ is the binding enthalpy (independent of protonation effects) and ΔH_{H+} is the enthalpic contribution of the protonation reaction.

Combining the two equations (11 and 12) gives (Jelesarov and Bosshard, 1999):

$$\Delta H_{app} = \Delta H'_{bind} + n_{H+} (\Delta H_{H+} + \Delta H_{buffer\ ionisation}) \quad (13)$$

So, for pH values where binding is independent of protonation (Jelesarov and Bosshard, 1999):

$$\Delta H_{app} = \Delta H'_{bind} \text{ as } n_{H+} = 0 \quad (14)$$

Thus, the use of various buffers is recommended if the buffer has not been previously characterised for protonation effects in order to asses the extent of this contribution. The

contribution of $\Delta H_{buffer\ ionisation}$ can be found either in already published tables or directly measured from ITC experiments (Baker and Murphy, 1996; Doyle *et al.*, 1995; Fukada and Takahashi, 1980).

1.1.3 Informational content of ITC data

Binding thermodynamics of a reaction, which characterises the molecular mechanism of binding and in more general terms characterising structure-function relationships, is a useful analytical tool (Doyle, 1997). Various parameters describe the binding thermodynamics and these are dealt with in more detail below.

1.1.3.1 Binding free energy

Binding free energy or Gibbs free energy (ΔG) is the global overall description parameter of the binding process as it characterises the stability of a given biological complex. The contributions to the parameter, ΔG, are dependant on the nature of the system under investigation (Perozzo *et al.*, 2004). The total binding free energy can be dissected into two major contributing terms. From equation (6) it can be seen that these terms are the enthalpy and the entropy of binding. However, these terms are meaningless unless equated to particular interactions or changes of state upon an occurrence of a process such as protein-ligand binding or protein folding/unfolding. To break it down further, contributions arise from the formation of secondary, tertiary and, if applicable, quaternary structure or formation of a protein-ligand complex. The complexation or folding processes utilise van der Waals interactions, hydrogen bonding, salt bridges and dipole-dipole interactions. Further, contributions arise from the solvation and desolvation of interacting surfaces, conformational transitions, loss of translational and rotational degrees of freedom and others, all of which bear the necessity to be accounted for on individual basis (Gohlke and Klebe, 2002; McGavin, 2004; Perozzo *et al.*, 2004; Sturtevant, 1977).

As a global parameter, ΔG is insensitive to the changes of ΔS and ΔH due to the fact that interacting systems tend to compensate the enthalpic and entropic contributions (Dunitz, 1995; Lumry and Rajender, 1970). This highlights the importance of understanding the entropy and enthalpy of a binding reaction.

1.1.3.2 Binding enthalpy

The observed heat effect of a binding reaction reflects a global property of the system under investigation and encompasses the total heat change in the calorimetric cell upon addition of ligand. Measured heat also contains contributions from nonspecific heat effects and there could be contributions from protonation effects coupled to binding. Thus, in order to determine solely the intrinsic binding enthalpy one needs to correct for the abovementioned contributions. Despite the corrections, the heat changes are still composed of different intrinsic contributions and this is the reason why the enthalpy is an apparent or observed (ΔH_{obs}) quantity (Jelesarov and Bosshard, 1999).

The physical meaning of ΔH represents the changes in noncovalent bond energy occurring during an interaction. The measured enthalpy is a result of formation and/or breaking of many individual bonds. It reflects the loss of protein-solvent bonds (including hydrogen bonds and van der Waals interactions), formation of protein-ligand bonds (including salt bridges and van der Waals contacts) and solvent reorganisation near protein surfaces. All these contribute either favourably or unfavourably and the resultant is likely to be smaller than the specific interactions (McGavin, 2004; Perozzo *et al.*, 2004).

A large part of the observed enthalpy change is due to bulk hydration effects where an enthalpic contribution of -16kJ/mol is placed on the transfer of a water molecule from the bulk phase into a binding protein (Gohlke and Klebe, 2002). In high resolution crystal structures, the presence of a water molecule(s) can be observed at the complex interface in order to improve complementarity between the interacting surfaces. However, the entropic penalty counterbalances such favourable enthalpies. An example is ANS-I-FABP complex formation, where ordering of both ANS (Kirk *et al.*, 1996) and a water molecule (Wiesner *et al.*, 1999) at the binding cavity results in unfavourable entropy.

All direct noncovalent bonds at the binding interface also contribute to ΔH. However, the dissection of such interactions is very difficult since the heat effect of a particular bond is a balance between the reaction enthalpy of the ligand to the protein and to the solvent. Further, any structural alterations at the binding site may contribute to the binding enthalpy (Jelesarov and Bosshard, 1999; Perozzo *et al.*, 2004).

1.1.3.3 Binding entropy

As can be seen from equation (6), ΔS can be directly calculated from ΔG and ΔH. The total entropy change is a sum of several contributing factors such as hydration effects and loss or gain of degrees of freedom of interacting species or solvent (Makhatadze and Privalov, 1996). Entropy of hydration is a major contributing factor to the ΔS of complex formation as values for hydration of polar and non-polar groups is substantial. Solvent is released upon burial of water-accessible surface area and its contribution is often large and positive to the total entropy of interaction. Unfavourable contributions often arise from the reduction in the degrees of freedom around torsion or dihedral angles of protein side-chains and ligand groups. An additional entropy term accounts for the reduction of the number of particles in solution and their degrees of freedom (Jelesarov and Bosshard, 1999; McGavin, 2004; Perozzo *et al.*, 2004; Sturtevant, 1977).

Usually when one tries to account for unfavourable contribution of entropy it can reflect various contributing factors. However, positive entropy change is a strong indicator that water molecules have been released from the complex surface (Jelesarov and Bosshard, 1999).

1.1.3.4 Heat capacity change

When ΔH is determined at a range of temperatures, the change in the heat capacity (ΔC_p) at constant pressure for an interaction can be measured by the slope of the linear regression analysis of the observed heat change plotted vs. temperature.

There is a strong correlation between ΔC_p and the change in water-accessible surface area of a protein at room temperature. A greater change in the ΔC_p value is accomplished via exposure of a nonpolar group to solvent during protein unfolding, than exposure of a polar group (Loladze *et al.*, 2001; Makhatadze and Privalov, 1990). That being the case, the opposite effect should be exhibited upon protein folding and protein-ligand complexation as protein (and ligand) surface is buried during these processes. Nonpolar groups raise the heat capacities of solutes in aqueous solutions. Cages of structured water with high heat capacities and low entropy are formed around the very same nonpolar groups in aqueous solution (Sturtevant, 1977). This correlation of heat capacity to

burial/exposure of surface area provides a link between thermodynamic parameters and structural information. Thus, the prediction of thermodynamic parameters has been made possible (Perozzo *et al.*, 2004).

1.1.3.5 Enthalpy-entropy compensation

The phenomenon of enthalpy-entropy compensation is characterised by linear relationship between the change in enthalpy and the change in entropy. Favourable changes in binding enthalpy are compensated by opposite changes in entropy and vice versa, resulting in small changes in binding affinity (equation (2)) and free energy over a range of temperatures. Previously thought of as 'ubiquitous property of water'(Lumry and Rajender, 1970), the enthalpy-entropy compensation is regarded as a more general property due to weak intermolecular interactions, where hydrogen bonding in aqueous solution is one of the cases. Thus, increased bonding results in favourable $\Delta H°$. However, it also results in increasing the orderedness of the interacting molecules and generating more unfavourable $\Delta S°$ (Dunitz, 1995). It is not surprising that these parameters are correlated as both of them are connected to ΔC_p (see equation (5)). In practical terms, the enthalpy-entropy compensation is the most difficult phenomenon to be overcome when the binding affinity of a compound to a protein has to be optimised in the field of rational drug design and medicinal chemistry (Perozzo *et al.*, 2004).

1.2 Glutathione *S*-transferase

Glutathione *S*-transferases or GSTs (EC 2.5.1.18), previously known as ligandins, are proteins which apart from their biological function of glutathione conjugation to electrophiles can bind endogenous and xenobiotic non-substrate ligands (Habig *et al.*, 1976). They play an important part in detoxification metabolism, and at least one hundred xenobiotic chemicals have been identified, which induce GSTs, thus regulating the proteins (Hayes and Pulford, 1995). Widely distributed in nature, GSTs are found in bacteria, yeast, molds, fungi, mollusks, crustaceans, worm parasites, frogs, insects, plants, fish, birds and mammals (Hayes and Pulford, 1995 and references therein). Mammalian GSTs have been grouped into several classes based on the degree of amino acid sequence identity (Hayes and Pulford, 1995). These classes include: Alpha, Mu, Pi (Mannervik *et*

al., 1985), Theta (Meyer *et al.*, 1991), Kappa (Pemble *et al.*, 1996), Sigma, Zeta (Board *et al.*, 1997) and Omega (Board *et al.*, 2000) GSTs.

1.2.1 Class Alpha glutathione transferase

Human glutathione *S*-transferase class alpha with two type 1 subunits found predominantly in the liver (Habig *et al.*, 1976) has a conserved overall folding topology.
It is a homodimer of approximately 50kDa and each subunit is made up of two domains. Domain I which is the smaller N-terminal domain (Figure 3), has an α/β-type core structure (Dirr *et al.*, 1994). Topologically it consists of βαβαββα structural motif, which despite the absence of sequence similarity, has an overall fold resembling that of the thioredoxin superfamily (Holmgren *et al.*, 1975). Domain II is the larger C-terminal domain (Figure 3) with an all-α-type core structure comprised of five amphipathic α-helices with an overall packing geometry of a right-handed spiral (Dirr *et al.*, 1994). Upon dimerisation 14 % of the previously exposed water-accessible surface area is buried at the subunit interface (Dirr *et al.*, 1994) and a hydrophobic cleft is formed at the dimer interface (Figure 4 (A)). The two subunits in the enzyme are related by a two-fold axis. There are predominantly hydrophobic intersubunit contacts between the structural elements in domain I of one subunit and domain II of the adjacent subunit, with an interesting conserved structural feature entailing the stacking together of two symmetrically equivalent arginine (Arg68) guanidino groups near the dimer two fold axis (Dirr *et al.*, 1994).
The distinguishing structural feature of hGST A1-1 among the rest of the GST classes is the presence of extra C-terminal residues forming an additional α-helix, the α9 helix. In the absence of substrates the α9 helix is mobile/disordered. The mobility/disorder of the α9 helix is a conclusion drawn from the lack of electron density for the feature in the apo enzyme (Cameron *et al.*, 1995; Sinning *et al.*, 1993). In the presence of a bound substrate or inhibitor the helix becomes ordered and encloses the H-site, forming a lid and providing a more hydrophobic environment for the bound molecule (Cameron *et al.*, 1995; Sinning *et al.*, 1993).The helix is important for the catalytic function of hGST A1-1

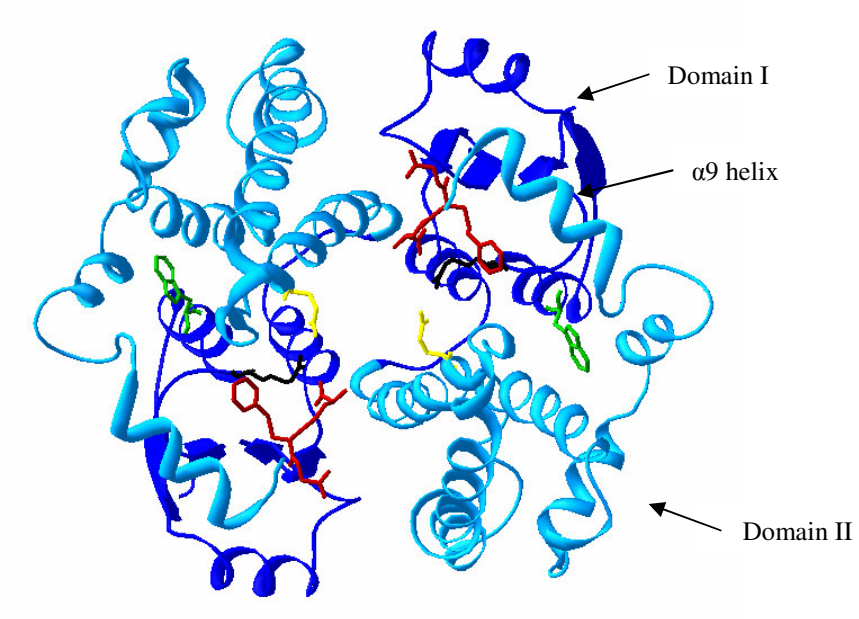


Figure 3 A ribbon representation of homodimeric hGST A1-1 as viewed down the two-fold axis (pdb code: 1guh; (Sinning *et al.*, 1993)). The protein is complexed with *S*-benzyl-glutathione (dark red). *S*-benzyl-glutathione is bound at the active site, with the glutathione moiety occupying the G-site and the benzyl moiety occupying the H-site. Arg15 (black), Glu104 (yellow) and Trp21 (green) are highlighted. α9 helix is shown immobilised over the H-site. The figure was generated using Swiss-Pdb Viewer (Guex and Peitsch, 1997).

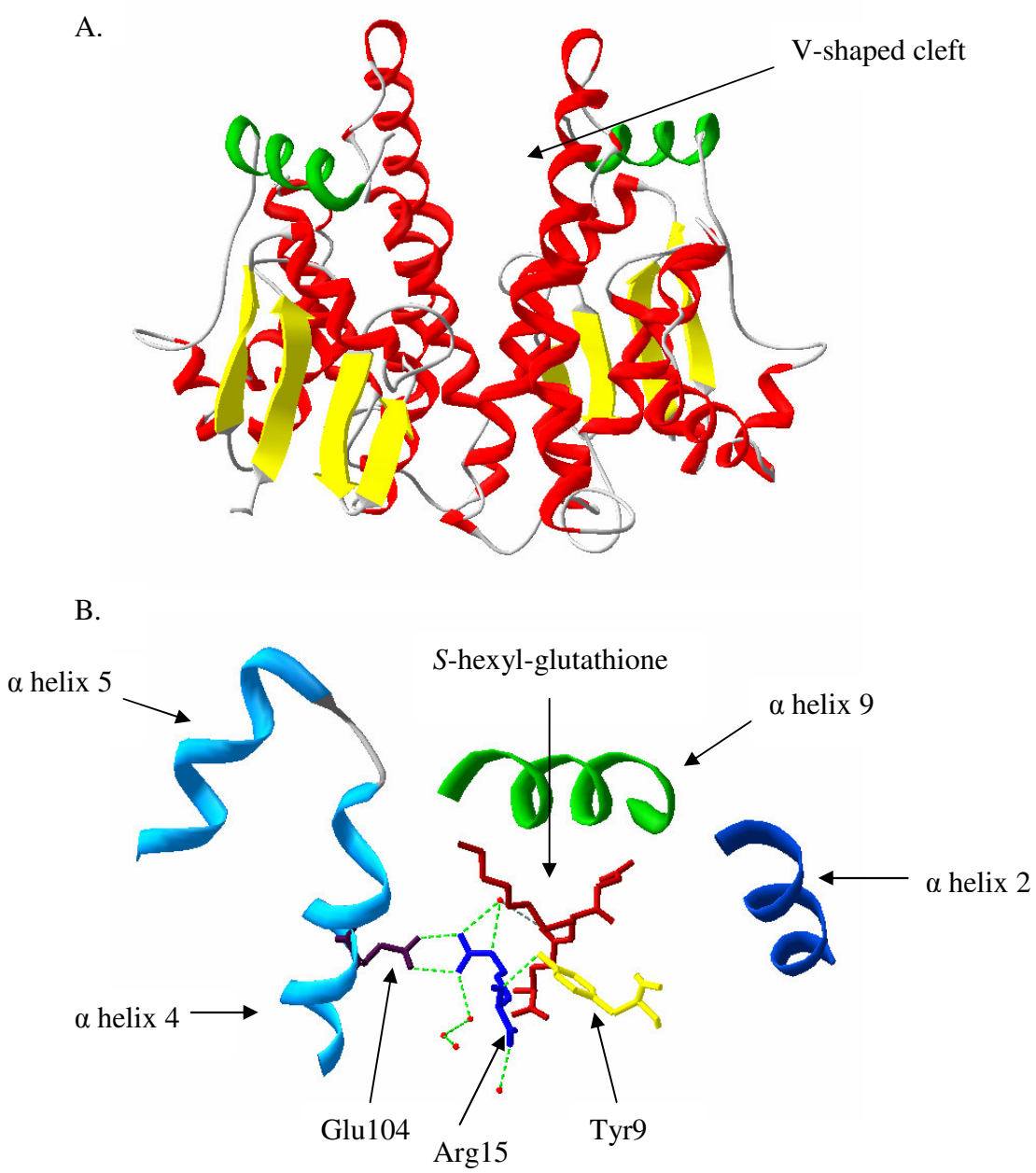


Figure 4. Ribbon representation of the crystal structure of hGST A1-1(pdb code 1k3l; (Le Trong *et al.*, 2002)). (A.) α helices are shown in red, β strands shown in yellow and the α9 helix is highlighted in green. The V-shaped cleft is indicated. (B.) shows the active site of the protein with helix 2 in dark blue, helix 9 in green, part of helix 4 and helix 5 in light blue, *S*-hexyl-glutathione in dark red, Glu104 in black, Arg15 in blue, and Tyr9 in yellow. The G-site is below and the H-site is above line linking Glu104-Arg15 and Tyr9. The H-site is occupied by the *S*-hexyl moiety in ball and stick representation. Dotted lines represent hydrogen bonds and red dots water molecules. The figure was generated using Swiss-Pdb Viewer (Guex and Peitsch, 1997)

and α9 helix immobilisation as well as stabilisation by forming a lid and providing a more hydrophobic environment for the bound molecule (Cameron *et al.*, 1995; Sinning *et al.*, 1993). The helix is important for the catalytic function of hGST A1-1 and α9 helix immobilisation as well as stabilisation by active site ligands enhances affinity for non-substrate ligands ANS and BSP (Dirr and Wallace, 1999). A C-terminal residue Phe222 was found to contribute to the binding of ANS by hGST A1-1, but not having an important role in regulating the dynamics of the C-terminus (Sayed *et al.*, 2002). Another residue Ile219 forms a part of the α9 helix of hGST A1-1 and is in close proximity to Ala38 of the α2 helix. The bulkiness of Ile219 prevents the α9 helix from flapping over the α2 helix. This in turn reduces accessibility of the binding site to the ligand as α9 helix forms a characteristic cap over the active site. Substitution of Ile219 with Ala rendered the helix even more mobile in the absence of ligand, but had no effect on the binding affinity of ANS (Kuhnert *et al.*, 2005; Mosebi *et al.*, 2003). In a recent study of a conserved N-cap residue Asp209 (the amino acid preceding α9 helix) was mutated to Gly in order to investigate Asp209 contribution to the stability and dynamics of the C-terminal region. There was perturbation of normal ligand-induced localisation of the region at the active site, thus resulting in a more solvent exposed and less hydrophobic H-site. The conformational dynamics of the C-terminal region was also altered, affecting the catalytic efficiency of hGST A1-1 (Dirr *et al.*, 2005).

1.2.2 Unfolding and stability of hGST A1-1

Equilibrium unfolding studies have been reported for a number of GSTs, including class Alpha (Wallace *et al.*, 1998b), class Pi (Dirr and Reinemer, 1991; Erhardt and Dirr, 1995) and Sj26GST (Kaplan *et al.*, 1997), which are consistent with a cooperative two-state unfolding mechanism. Moreover, stopped-flow kinetic studies done by (Wallace *et al.*, 1998b) have indicated the existence of a three-state kinetic unfolding mechanism involving the folded dimer and the unfolded monomer for hGST A1-1. The transition state was proposed to represent a native dimer or dimeric intermediate (Wallace *et al.*, 1998b). Further studies done with hGST A1-1 have indicated a four-step kinetic model accommodating the dynamics of the C-terminal α9 helix (Dirr and Wallace, 1999). The helix 9 changes conformation from stable to mobile to "coil" in the presence of

increasing urea concentrations. The stable conformation is only applicable to physiological conditions in human cells as the stabilisation is due to a bound ligand (Dirr and Wallace, 1999). The latest studies incorporated the above two kinetic unfolding proposals by redefining the transient dimeric species as species undergone structural changes at the interdomain interface near Trp21 and a result of destabilization/unfolding of helix9 (Wallace *et al.*, 2000). Conformational studies on the class Mu (Hornby *et al.*, 2000) and Sigma (Stevens *et al.*, 1998) enzymes, however, are suggestive of a multi-state equilibrium pathway involving stable monomeric intermediates. The class Sigma GST displays a complex unfolding pathway which includes the presence of both thermodynamically stable dimeric and monomeric species (Stevens *et al.*, 1998).

1.2.3 Active site

At each end of the V-shaped cleft, spanning the dimer interface of hGST A1-1, there is an active site. Each of the two active sites of the dimer has two regions, for binding specifically the physiological substrate glutathione (the G-site) and for binding hydrophobic electrophilic molecules (the H-site) (Sinning *et al.*, 1993). The location and description of the active site is made possible by the availability of crystal structures of hGST A1-1 in complex with glutathione conjugates (Cameron *et al.*, 1995; Le Trong *et al.*, 2002; Sinning *et al.*, 1993). Thus, key residues involved in substrate recognition can be identified.

1.2.3.1 Glutathione binding site

The G-site (highly specific for glutathione (GSH)) involves a network of specific polar interactions between the tripeptide, domain I of one subunit and domain II of the other subunit (Figure 5). In the structure of hGST A1-1•*S*-benzyl-glutathione, the glutathione tripeptide adopts an extended conformation. Most of the interactions between GSH and hGST A1-1 come from domain I. However, salt links at both ends of the tripeptide are formed with two residues (Asp101 and Arg131) from domain II (Sinning *et al.*, 1993). The sulphur atom of glutathione forms two close contacts with the hydroxyl group of Tyr9 and to the N^{ε} of Arg15, and both of these interactions are essential for the hGST A1-1 catalysis (Sinning *et al.*, 1993). Residues contributing to the binding of GSH are

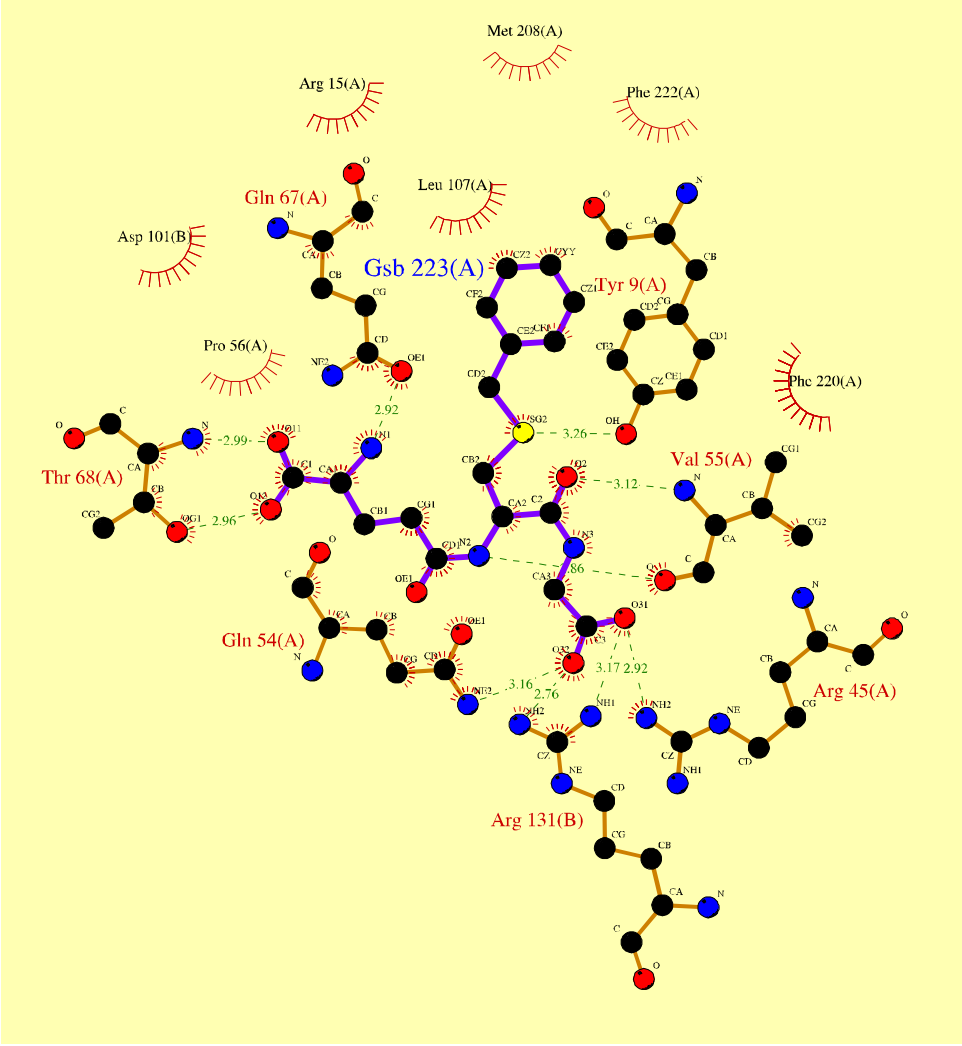


Figure 5 Schematic representation of bound *S*-benzyl-glutathione in the G-site of hGST A1-1. The residues involved in the interactions with the inhibitor form either salt links or hydrogen bonds. This figure was generated via the program, LIGPLOT (Wallace *et al.*, 1995).

conserved within a gene class. Between GST classes the residues are either conserved or conservatively replaced and differences in hydrogen bonding interactions have been reported. There is salt link formed between Arg15 and Glu104, which stabilises the protein conformation at the G-site for hGST A1-1. However, in class Mu, Arg15 is replaced by a topologically equivalent residue Leu. Despite these differences the orientation of the glutathione moiety is similar in all classes (Dirr *et al.*, 1994).

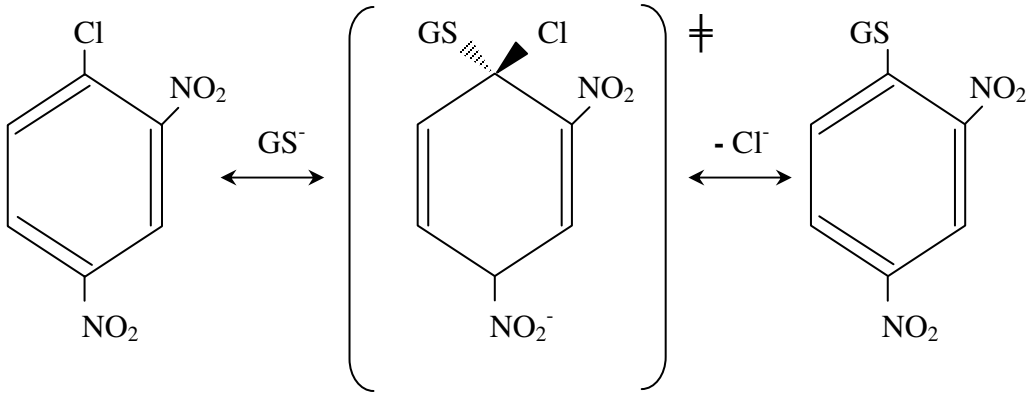
1.2.3.2 Hydrophobic substrate binding site

In crystal structures of hGST A1-1 (Cameron *et al.*, 1995; Dirr *et al.*, 1994; Le Trong *et al.*, 2002; Sinning *et al.*, 1993) the moiety which is covalently attached to glutathione sulphur atom is located in the H-site. For example, the benzyl group of *S*-benzyl-glutathione is located at the H-site. More specifically, it is confined by three regions: the N-terminus of α1 (Phe10, Ala12, the methylene group of Arg13, Gly14 and the methylene group of Arg15); the C-terminus of α4 (Leu107, Leu108, Pro110, Val111 and the side chain of Glu104 salt linking to the Arg15); the region immediately prior to and all of the one edge of α9 (Met208, Leu213, Ala216, Phe220, and Phe222) (Sinning *et al.*, 1993). This results in a highly hydrophobic pocket. The formation of such hydrophobic surface exposed to solvent in the absence of H-site substrates, is a result of such clusters of hydrophobic side chains. The differences in topology among gene classes allows the H-site to accommodate a variety of hydrophobic electrophilic substrates of different size and polarity (Dirr *et al.*, 1994). The binding of ethacrynic acid-glutathione (EA-GSH) to hGST A1-1 has the same hydrogen-bonding interactions as described for the crystal structure of *S*-benzyl-glutathione. However, EA-GSH exhibits two conformations at the active site of hGST A1-1 (Cameron *et al.*, 1995). Two different conformations in the H-site of hGAT A1-1 has also been reported for bound *S*-hexyl moieties of *S*-hexyl glutathione. This was argued to be the result of the absence of specific interactions and sufficient space in the binding pocket for multiple conformations of this side chain. (Le Trong *et al.*, 2002). An interesting observation was made for the crystallisation of rGST A1-1 variant W21F/F220Y. In the presence of glutathione sulphonate (GSO_3^-), Arg15 no longer forms a salt bridge with Glu104 and the localised α9 helix adopted a different conformation

relative to hGST A1-1 α9 helix. However, all G-site interactions are conserved for the glutathione moiety of GSO_3^-, and the ligand itself is well-ordered. (Adman *et al.*, 2001). Clearly, substrate specificity plays a more important role in the G-site than it does in the H-site due to the accommodation of structurally different hydrophobic substrates (Dirr *et al.*, 1994).

1.2.3.3 Catalytic mechanism

The GSTs catalyse a reaction involving nucleophilic addition of reduced glutathione (GSH) to a variety of electrophilic compounds, including aryl chloride such as CDNB. A typical conjugation reaction bears superficial resemblance to S_N1 and S_N2 reaction mechanisms. However, it appears by neither of those. Nucleophilic aromatic substitutions proceed by an addition/elimination mechanism, where the attacking nucleophile (GSH) first adds to the electron-deficient aryl chloride (CDNB), forming a negatively charged intermediate called Meisenheimer complex. The chloride ion is then eliminated in the second step (McMurry, 1996). An example of the reaction mechanism is given in Figure 6. Glutathione is believed to bind first under physiological conditions as GSH concentration is between 1 and 10mM in normal cells, which is at least three orders of magnitude higher than its dissociation constant (Wilce and Parker, 1994). Central to the mechanism appears to be the formation of a hydrogen bond between Tyr9 in the active site of hGST A1-1 and the thiol sulphur of GSH (Figure 4 (B)) (Bjornestedt *et al.*, 1995; Graminski *et al.*, 1989). Site-directed mutagenesis studies have been used to assess the importance of Tyr9. The residue was mutated to phenylalanine, which adversely affected the hGST A-1 CDNB-conjugating activity, thus confirming Tyr9 importance in catalysis (Allardyce *et al.*, 1999; Stenberg *et al.*, 1991b). Another residue, Arg15, has been shown to contribute to the catalytic activity of hGST A1-1 (Bjornestedt *et al.*, 1995). Mutagenesis studies have indicated the importance of Arg15 in binding and activation of glutathione. The residue is believed to create an electrostatic potential in the G-site which favours ionisation of GSH bound to hGST A1-1 (Bjornestedt *et al.*, 1995).



1-chloro-2,4-dinitrobenzene **1-chloro-1-(*S*-glutathionyl)-2,4-dinitrobenzene** **1-(*S*-glutathionyl)-2,4-dinitrobenzene**

Figure 6. A schematic representation of GST catalysed conjugation of glutathione to CDNB. Within brackets is the Meisenheimer complex in which the sulphur atom and the chloride are linked to the same carbon. Adapted from (Widersten *et al.*, 1996).

1.2.4 Non-substrate ligand binding site

To date there is no crystal structure available for hGST A1-1 bound to a non-substrate ligand. However, there have been numerous attempts to identify the location of this ligand-binding site. Sluis-Cremer *et al.* (1996) identified a possible site for ANS and aflatoxin B1 (AFB_1) by means of fluorescence-resonance energy transfer (FRET). The location was proposed to be at the dimer interface near the dimer two fold axes in the V-shaped cleft (see Figure 4 (A)). It was also proposed that one molecule of ANS or AFB_1 binds hGST A1-1 dimer. A more recent study looked at a chemically modified Cys 112, in order to asses the binding of non-substrate ligands. Cys 112 is a residue adjacent to the H-site whose side chain thiol group projects into the subunit interface cleft (Lyon and Atkins, 2002) The study indicated that the non-substrate ligand binding site is not located at the intersubunit cleft for the ligands probed as there was no effect on the binding of the same (Lyon and Atkins, 2002). The location of the L-site has been proposed by Le Trong *et al.* (2002) to be located in a region below the mobile elements of helix 9 and the alpha 4-5 linking region (Figure 3(B)). The most recent studies, however, place the bound ANS in the H-site of hGST A1-1 (Dirr and Wallace, 1999; Dirr *et al.*, 2005; Sayed *et al.*, 2002)

1.2.5 R15L hGST A1-1 variant

Arg15 has a very characteristic feature in hGST A1-1. N^{ε} of Arg15 forms a hydrogen bond with the sulphur atom of GSH derivatives, thus, participating in the binding of the substrate. Additional structural features of the amino acid side chain include hydrogen bonding of the backbone NH to the phenolic group of Tyr9 (Figure 4(B)). The methylene groups of Arg15 contribute to the hydrophobic binding in the H-site and the guanidino group forms a salt link with Glu104 carboxylate side chain (Bjornestedt *et al.*, 1995; Sinning *et al.*, 1993).

A decrease in specific activity towards CDNB, cumene hydroperoxide and androstenedione was exhibited, when Arg15 was substituted by Lys, Leu, Ala or His (Stenberg *et al.*, 1991a). The results are summarised in Table 1. The R15L substitution retains the positive charge and Lys side chain NH_3^+ can interact with either the thiolate of GSH or Glu104.

Table 1. Specific activity of hGST A1-1 and eight Arg variants for three substrates.

Protein/ substrate	CDNB	Cumene hydroperoxide	Androstenedione
	Specific activity (μmol min^{-1} mg^{-1})		
GST wt	75/60.2*±3.0	9/ 10.2*±0.5	12/ 12.1*±0.8
Arg13Ala	7.9±0.9*	3.0 ±0.2*	1.5±0.1*
Arg20Ala	8.9 ± 0.8*	19.7 ±1.4*	9.7 ±0.6*
Arg69Ala	15.4±0.8*	7.2±1.8*	1.7 ±0.2*
Arg187Ala	32.3 ±1.1*	6.3 ±0.6*	3.8 ±0.2*
Arg15Ala	0.4	0.08	0.1
Arg15His	0.2	0.07	0.08
Arg15Lys	25	3.4	2.6
Arg15Leu	3.1	0.12	1.2

* Values taken from Stenberg *et al.*, (1991); all other values are taken from Bjornestedt *et al.*, (1995).

Table 2 . IC_{50} values for various inhibitors of hGST A1-1 and Arg variants of the protein

Protein/ inhibitor	[BSP]	[GS-EA]	[Hematin]	[Triethyl bromide]	[*S*-hexyl-glutathione]	[*S*-benzyl-glutathione]
	IC_{50} (μM)					
GST wt	7* / 10.6	1.0	0.07	10.9	0.7 */ 1.2	7.0
Arg13Ala	3*	--§	--	--	0.4*	--
Arg20Ala	0.2*	--	--	--	0.1*	--
Arg69Ala	0.2*	--	--	--	0.03*	--
Arg187Ala	7*	--	--	--	0.4*	--
Arg15Ala	14.5	3.1	0.9	30	7.2	33.9
Arg15His	46.3	10.3	3.4	387	22.3	131
Arg15Lys	6.9	0.2	0.04	15.6	22	16.3
Arg15Leu	38.3	0.2	1.5	2.7	0.5	11.3

* values taken from Stenberg *et al.*, 1991; the rest of the values are taken from Bjornestedt *et al.*, (1995); § No data available

Upon substitution of Arg15 with Leu the volume is essentially maintained but the charge is lost and the R15A substitution results in loss of all interactions with the substrate. The last replacement by His looked at the importance of the basic side chain for the catalytic function, as well as introduction of a bulky aromatic side chain in the active side. The results from the inhibition studies performed are given in Table 1 (Bjornestedt *et al.*, 1995). Earlier studies on conserved Arg residues 13, 20, 69 and 187 of hGST A1-1, which were substituted with Ala exhibited a decrease in the specific activities towards CDNB, cumene hydroperoxide and androstenedione. For comparative purposes the results from the enzyme assays as well as inhibition studies are presented in Table 1 and 2, respectively (Stenberg *et al.*, 1991a).

The Arg13 guanidino group is on the edge of the dimer interface and in close proximity to the binding site for class alpha, but not in the 4Å radius of glutathione so as to participate directly in ligand binding. Arg20 is in close proximity to Arg15 and it forms salt links with glutamic acid residues at positions 17 and 32. It is possible that structural changes occur, accounting for the decrease in specific activity. Arg69 and 187 are 20Å and 40Å from the active site, thus having no direct participation in the binding process. They also do not form part of any domain interface (Le Trong *et al.*, 2002; Sinning *et al.*, 1993). Arg15, on the other hand, is located in the 4Å radius of the substrate. Involvement in binding for Arg15 is indicated by the reduced specific activity of the generated variants (Table 1) as well as reduced affinity (Table 2) for the substrates. Arg15 has the lowest value for specific activity and the highest value for IC_{50} in comparison to the rest of the Arg to Ala substitutions (Tables 1 and 2).

It appears that incorporating an aromatic ring in the active site (variant R15H) is far more disruptive than reducing the charge and bulk of the of Arg15 side chain (Bjornestedt *et al.*, 1995; Stenberg *et al.*, 1991a).

Objectives

Arg15 has unique structural and functional characteristics in the active site of hGST A1-1 (Figure 4(B)). The sulphur atom of *S*-hexyl-glutathione in the active site of the enzyme is within hydrogen-binding distance of N^{ε} of Arg15 as well as the hydroxyl group of Tyr9 (Le Trong *et al.*, 2002). The ionic interaction between Arg15 and the thiol sulphur of GSH in alpha class GSTs has no counterpart in the Pi and Mu classes (Dirr *et al.*, 1994; Wilce and Parker, 1994). The catalytic importance of Arg15 was established via comparison of Tyr → Phe variants in Alpha, Pi and Mu. The mutation reduced the catalytic activity of the enzymes by approximately two orders of magnitude. However, the percentage activity remaining of the Tyr → Phe variants in class alpha human and rat enzymes was approximately tenfold higher than the corresponding mutants from the other classes (Bjornestedt *et al.*,and references therein). Despite the fact that the catalytic importance of Arg15 is established, little is known about the effect on the binding of glutathione conjugates and nonsubstrate ligands. It has been argued by Matulis and Lovrien (1998) that binding of the nonsubstrate ligand ANS to few proteins is accomplished via ion pair formation with a charged residue such as Arg. This notion has been shown to be applicable for variety of ANS binding proteins (Lartigue *et al.*, 2003; Ory and Banaszak, 1999; Schonbrunn *et al.*, 2000). For I-FABP the proposed mechanism of binding involves initial attraction of the sulphonate moiety of ANS to the site forming and ion pair with Arg106. This is followed by the accommodation of the aryl rings of ANS at the binding site. (Kirk *et al.*, 1996). Class alpha GSTs are no exception. Recent studies place ANS in the H-site of hGST A1-1 (Dirr *et al.*, 2005), and molecular docking done with ANS indicates that Arg 15 is in hydrogen bonding distance of the ligand. The importance of the positive charge provided by the Arg15 side chain in the active site of hGST A1-1 is addressed by performing a mutational study. To characterise the thermodynamics of complexation, ligands ANS and GSO_3^- were used to bind to R15L variant.

Additional structural features displayed by Arg15 include: a hydrogen bond supplied by backbone NH of Arg15 to the phenolic hydroxyl group of Tyr9; Arg15 methylene groups located in the active site, contributing to the binding at the hydrophobic binding site (H-site); and a guanidino group forming a salt link with the side-chain carboxylate of

Glu104. Arg15 is a conserved residue among the alpha class sequences with the exception of chicken liver GST, where the residue is substituted with Lys (Chang *et al.*, 1992; Dirr *et al.*, 1994). Glu 104 is also preserved in the majority of the Alpha Mu and Pi known sequences with the exception of rGST A3 where the residue is replaced by Met (Dirr *et al.*, 1994). However, the importance (or lack thereof) of this additional structural feature (Arg15-Glu104 salt link) at the interdomain interface has not been addressed previously. The conformational stability study was aimed at addressing the impact which the interaction has at the interdomain interface.

Chapter 2
Experimental procedures

2.1 Materials

8-Anilino-1-naphthalene sulphonate (ANS) and 1-chloro-2,4-dinitrobenzene (CDNB) were purchased from Sigma (St. Louis, MO, USA). Reduced glutathione (GSH) was from ICN Biomedicals, Inc (Aurora, Ohio, USA). Ultrapure urea was from Merck (Darmstadt, Germany). The QuikChange™ Site-directed Mutagenesis kit was purchased from Stratagene (La Jolla, CA, USA; (Papworth *et al.*, 1996)). The pKHA1 plasmid was a gift from Prof. B. Mannervik (Uppsala University, Uppsala, Sweden; Stenberg *et al*., 1992). All other reagents were of analytical grade.

2.2 Construction of the R15L variant by site-directed mutagenesis

2.2.1 Oligonucleotide primer design

In order to design the oligonucleotide primers, the software package, GeneRunner v.3.04 was utilised. The design of primers was in accordance with the published nucleotide sequence for hGST A1-1 (Stenberg *et al.*, 1992). Primers were also designed in accordance with the specifications given for the usage of QuikChange™ Site-directed mutagenesis kit (Stratagene; (Papworth *et al.*, 1996)). The oligonucleotide primers used to create the R15L hGST A1-1 had the following sequences:

R15L Forward primer: 5′- AAT GCA CGG GGC **TTA** ATG GAG TCC ACC -3′

and

R15L Reverse primer: 5′- GGT GGA CTC CAT **TAA** GCC CCG TGC ATT -3′.

The bold trinucleotide represent the mutation which generates the variant R15L.

2.2.2 Site-directed mutagenesis

The R15L mutant was generated using the QuikChange™ site-directed mutagenesis kit (Papworth *et al*., 1996). Double-stranded pKHA1 (Stenberg *et al.*, 1992) DNA was used as the template DNA for the mutagenesis experiments. The sample reactions were

performed in a total volume of 50 µl containing ~20 ng of double stranded DNA template, 125 ng of each mutagenic primer, 10 mM dNTP mix and 10 x reaction buffer (100 mM potassium chloride, 100 mM ammonium sulphate, 200 mM Tris-HCl, pH 8.8, 20 mM magnesium sulphate, 1% Triton® X-100, 1 mg/ml nuclease-free bovine serum albumin; supplied with kit). *PfuTurbo* DNA polymerase (2.5 U/µl) was also added to the reaction mixtures. The thermal cycling parameters used to generate the mutant products were: 16 amplification cycles of 30 seconds at 95°C to denature the DNA, 60 seconds at 56°C to anneal the primers to the single stranded DNA template and 5 minutes at 68°C for DNA extension. The sample reaction mixtures were treated with *Dpn*I (10 U/µl; Stratagene, USA) for one hour at 37°C, in order to digest the methylated, nonmutated parental DNA template. The daughter DNA strands were then allowed to anneal for one hour at 20°C (this represents an additional step in the mutagenesis procedure). The *Dpn*I-treated DNA from each reaction mixture was then used to transform *Escherichia coli* XL1-blue supercompetent cells (Stratagene, USA).

The colonies of *Escherichia coli* XL1-blue supercompetent cells on LB (containing 100 µg/ml ampicillin) plates were replated and a duplicate plate with the abovementioned colonies was sent for sequencing (Inqaba Biotechnical Industries (Pty) Ltd). The sequencing service included extraction of the DNA from the *Escherichia coli* XL1-blue supercompetent cells.

2.2.3 Sequencing of the mutant plasmid DNA

cDNA encoding R15L mutant enzymes was sequenced to confirm the incorporation of the mutations into the pKHA1 plasmid. DNA sequencing was performed by Inqaba Biotechnical Industries (Pty) Ltd (Pretoria, South Africa; www.inqaba.com) using the BigDye® Terminator v3.1 Cycle Sequencing Kit from Applied Biosystems (Foster City, CA, USA) and a SCE 2410 Genetic Analyser from Spectrumedix (State College, PA, USA).

2.3 Overexpression and purification of wild type and R15L

The wild-type and R15L plasmids were transformed into competent *Escherichia coli* BL21 (DE3) cells. A 0.1 ml aliquot of cells was transferred into a prechilled

polypropylene tube, mixed with 1 µl (100 pg) of wild-type or mutant pKHA1 plasmid DNA. The cells were heat shocked for 30 seconds at 42°C and incubated on ice for 30 min. 0.9 ml of LB broth was added, and cells were grown at 37°C with shaking (250 rpm) for 1 hour to allow expression of the antibiotic-resistance gene. Transformants were selected by plating cells on LB agar plates with ampicillin (100 µg/ml) after incubation at 37°C for 17-20 hours.

2.3.1 Induction studies

In order to optimise the concentration of inducer for the expression of hGST A1-1 variant protein R15L, studies utilising isopropyl-β-D-thiogalactoside (IPTG) were performed. The inducer used was due to the fact that hGST A1-1 is over-expressed under the control of the Lac promoter in the pKHA1 plasmid. Thus, stationary phase *Escherichia coli* BL21 (DE3) cells were used to innoculate LB media supplemented with 100 µg/ml ampicillin. The cells were grown at 37 ºC to mid-log phase (A_{600} ~ 0.9; previously determined from a growth curve). IPTG was then added to the cultures to different final concentrations (0.2-1.0 mM) to induce the over-expression of the hGST A1-1 variant protein. From the time of induction, whole cell aliquots were removed from the cultures hourly, for the span of 16 hours. The samples were subsequently assessed by SDS/PAGE according to the method of Laemmli (1970; see section 2.2.4).

2.3.2 Overexpression and purification

A primary culture of *Escherichia coli* BL21 (DE3) cells was grown overnight in LB broth in the presence of 100 µg/ml ampicillin. LB cultures containing 100 µg/ml ampicillin was inoculated with an overnight stationary phase culture of *Escherichia coli* BL21 (DE3) cells containing the wild-type and variant plasmid. Secondary culture of *Escherichia coli* BL21 (DE3) shaken at 250 rpm at 37°C was grown until the absorbance was in the range of 0.6-0.9. IPTG was added to a final concentration of 0.6 mM to induce the over-expression of the proteins (either wt or R15L) and cultures were incubated overnight. The cells were harvested by centrifugation (5000x*g* for 20 minutes) and resuspended in 8 ml of resuspension buffer, 10 mM sodium phosphate, 1 mM EDTA and 0.02 % sodium azide, pH 7.0. The resuspended cells were frozen at –20°C in the presence of lysozyme

for at least two hours to promote cell lysis. The cells were disrupted briefly via sonication and then centrifuged at 13 000 rpm for 20 minutes at 4°C. The wild-type and R15L mutant proteins were purified from *Escherichia coli* BL21 (DE3) cells using CM-Sepharose cation exchange chromatography. The supernatant containing cytosol was then applied to the CM-Sepharose column pre-equilibrated with the resuspension buffer. The column was washed with at least 10 column volumes of the resuspension buffer until the unbound protein was eluted. The protein was then eluted using a linear 200 ml salt gradient of 0-0.3 M NaCl prepared in 10 mM sodium phosphate buffer, 1 mM EDTA, 0.02% sodium azide, pH 7.0. The absorbance at 280 nm of the column eluent was monitored and detected protein fractions with A_{280} readings above 0.3 AU were electrophoresed on a 15% polyacrylamide gel SDS-PAGE (Laemmli, 1970) in order to assess the content and purity. Selected fractions containing pure protein were then pooled and concentrated by ultrafiltration through an Amicon PM-10 membrane on ice. The concentrated protein solution was buffer exchanged using Sephadex G-25 equilibrated with 20 mM sodium phosphate, pH 6.5, 100 mM NaCl, 1 mM EDTA, 0.02 % sodium azide.

2.3.3 Protein concentration determination

The concentrations of the hGST A1-1 and R15L proteins were determined spectrophotometrically using the Beer-Lambert Law:

$$A = \varepsilon_{\lambda} c l \qquad (15)$$

where A is the absorbance, ε is the molar extinction coefficient at a given wavelength λ, c is the molar concentration and l is the path length in centimetres. The molar extinction coefficient (ε) at 280 nm was calculated as follows (Perkins, 1986):

$$\varepsilon\ (M^{-1}\ cm^{-1}) = 5550\ \Sigma\text{Trp residues} + 1340\ \Sigma\text{Tyr residues} + 150\ \Sigma\text{Cys residues} \qquad (16)$$

The concentration of each protein, in the dimeric form, was therefore determined using a molar extinction coefficient at 280 nm (ε_{280}) of 38200 $M^{-1}\ cm^{-1}$.

The protein concentration was corrected for light scattering (Winder and Gent, 1971). A spectrum of the protein was obtained between 240 and 370 nm. Absorbance values were taken between 320 and 370 nm at 2nm intervals. These values were plotted against the wavelength values to obtain a linear fit. The absorbance value obtained from the extrapolated line at 280 nm was subtracted from the absorbance at this wavelength in order to obtain the corrected absorbance in the absence of scattering.

2.3.4 Sodium dodecyl sulphate polyacrylamide gel electrophoresis

The homogeneity and purity of the proteins was assessed by separation on 15 % SDS-PAGE (Laemmli, 1970). SDS/polyacrylamide separating gels of 15% acrylamide and 0.4% bisacrylamide and stacking gels of 5% acrylamide and 0.1% bisacrylamide were prepared. The protein samples were diluted five-fold in 5x loading buffer (0.5 mM Tris-HCl, pH 6.8, 20% (v/v) glycerol, 10% (w/v) SDS, 100 mM β-mercaptoethanol, 0.05% (w/v) bromophenol blue) and boiled for 5 minutes before loading onto the gels. The gels were run at 180 volts for 2 hours. Coomassie Blue (0.25% Coomassie Brilliant Blue R250 in 45% methanol and 10% acetic acid) was used to stain the gels for 1 hour. This was followed by destaining in destain solution (85% water, 15% acetic acid and 10% ethanol). The SDS/PAGE molecular mass markers used were: phosphorylase b (97 kDa), albumin (66 kDa), ovalbumin (45 kDa), carbonic anhydrase (30 kDa), trypsin inhibitor (20.1 kDa) and α-lactalbumin (14.4 kDa).

2.4 Steady-state kinetics

2.4.1 Enzyme assay

The enzyme activity of the wt and R15L was monitored spectrophotometrically at 340 nm in 0.1 M sodium phosphate, 1 mM EDTA, pH 6.5 (Habig and Jakoby, 1981) by measuring the formation of *S*-2,4-dinitrophenyl glutathione (ε = 9600 $M^{-1}cm^{-1}$), using final concentrations of 1 mM reduced glutathione (GSH) and 1 mM 1-chloro-2,4-dinitrobenzene (CDNB) in 3% (v/v) ethanol as substrates. GSH was initially added and then CDNB to give a 3 ml assay volume. The reactions in standard enzyme conditions were performed at room temperature (typically 20°C) and followed for 30 seconds, with

the standard error between assays allowed to be within 10 %. A Hewlett Packard model 8452A-diode array spectrophotometer was used. Blank assay rates with no enzyme were subtracted from the enzymatic rates. All reaction progress curves were linear.

2.4.2 BSP inhibition

The binding of the inhibitor bromosulphophthalein was determined to assess the effect of the replacement of R15L on the enzyme activity of human GST A1-1 using the standard enzymatic assay conditions described in section 2.3.1. The inhibition of bromosulphophthalein (0-90μM) was assessed by measuring the concentration of the respective ligand required to inhibit 50 % of the enzyme activity (IC_{50}).

2.5 Spectroscopic studies

2.5.1 Spectra determination

The fluorescence spectral properties of the wt and R15L variant protein were measured using 2 μM protein concentrations. Samples of both proteins in the presence or absence of 200 μM ANS were prepared. The experiments were carried out in 20 mM sodium phosphate buffer, pH 7, containing 1 mM EDTA and 0.02% sodium azide. Intrinsic tryptophan fluorescence emission spectra of the native proteins were obtained by selectively exciting the tryptophan residue at 295 nm. Fluorescence resonance energy transfer was used to monitor the protein bound ANS emission spectra. The excitation was also at 295nm and the fluorescence resonance energy transfer was from the tryptophan residue to ANS. The emission spectra were measured at 20^{o}C using a Perkin Elmer luminescence spectrometer LS50B. The excitation and emission bandwidths were set at 4 nm and the emission spectra were collected at a scan rate of 200 nm/minute. The spectra were corrected for buffer effects.

2.5.2 Unfolding studies

2.5.2.1 Reversibility of unfolding

In order to assess the conformational stability of a protein, the reversibility of the unfolding event needs to be established. The refolding of 2 μM protein samples incubated in 8 M urea was achieved by the ten-fold dilution of each sample reaction with buffer (20 mM sodium phosphate buffer containing 1 mM EDTA and 0.02% sodium azide, pH 6.5). Fluorescence emission spectra for the refolded proteins (0.2 μM protein in 0.8 M urea)

were compared to control emission spectra in which equivalent concentrations of protein and denaturant were used (i.e., 0.2 μM protein in 0.8 M urea).

2.5.2.2 Urea-induced equilibrium unfolding

Equilibrium unfolding studies were performed at 20°C in 20 mM sodium phosphate buffer, pH 6.5, containing 1 mM EDTA and 0.02% sodium azide. Fresh 10 M urea stock solutions (analytical grade) were prepared weekly and stored at 4°C. The molarity of the urea stock solutions was checked by refractometry before use (Pace, 1986).

Protein samples (2 μM) were incubated with urea (0-8 M) for at least one hour in order to achieve equilibrium. The sample reactions were subsequently analysed using far-UV CD and tryptophan fluorescence.

The extent of Rayleigh scattering due to aggregation throughout the unfolding process was monitored for the variant protein. This was done by setting the excitation and emission wavelengths at 295 nm.

2.5.2.3 Two-state fitting model for the unfolding transitions ($N_2 \leftrightarrow 2U$)

The unfolding transition curves of the wt and R15L variant protein are characterised by single sigmoidal transitions, suggesting the absence of any thermodynamically stable intermediates. The unfolding curves of the variant proteins were, therefore, analysed according to the two-state assumption (Pace *et al.*, 1989) in which the folded (N_2) and unfolded (U) conformational states are assumed to exist in significant concentrations within the equilibrium unfolding transition region. A two state fitting model ($N_2 \leftrightarrow 2U$) script designed by Diane Kuhnert and Henry Luo was utilized to fit the data (http://www.wits.ac.za/mcb/bcb/). The script is an executable fitting function of SigmaPlot v.8.0. The background for the fitting function used is given below.

Using this two-state assumption, the measured spectroscopic signal (Y_{OBS}) of each protein was converted to the fraction of the protein in the unfolded conformation (F_U). The fraction of the protein in the folded (F_F) and the unfolded (F_U) conformational states can be represented by:

$$F_F + F_U = 1 \qquad (17)$$

The observed property at any point in the equilibrium unfolding curve is therefore:

$$Y_{OBS} = Y_F F_F + Y_U F_U \quad (18)$$

where Y_F and Y_U are the values of the folded and unfolded conformational states, respectively. The Y_F and Y_U values were estimated from the linear extrapolation of the pre- and post- transition baselines observed in the equilibrium unfolding curves. The pre- and post- transition baselines can be described by the straight line equations $Y_F = ax + c$ and $Y_U = ax + c$, respectively. By combining these equations, we get:

$$F_U = (Y_N - Y_{OBS}) / (Y_N - Y_U) \quad (19)$$

The equilibrium unfolding constant, K_U, for the two-state transition model of dimeric proteins (Bowie and Sauer, 1989; Pace *et al.*, 1989) was then calculated using each point in the transition region as follows:

$$K_U = [U]^2 / [N_2] = 2P_t [F_U^2 / (1 - F_U)] \quad (20)$$

where P_t is the subunit protein concentration and F_U is the fraction of the protein in the unfolded conformation. Using equation (7), the Gibbs free energy change of unfolding for each reaction was determined:

$$\Delta G = -RT \ln K_U \quad (21)$$

The linear dependence of the Gibbs free energy change of unfolding on the denaturant concentration (Pace, 1986; Pace *et al.*, 1989) was then assumed in order to obtain values for $\Delta G(H_2O)$ and the *m*-value. The data was plotted and analysed according to the following equation (Pace, 1986; Pace *et al.*, 1989):

$$\Delta G = \Delta G(H_2O) - m[\text{denaturant}] \quad (22)$$

where $\Delta G(H_2O)$ is the difference in Gibbs free energy between the folded and unfolded protein in the absence of denaturant (Pace *et al.*, 1989) and *m* represents the dependence of free energy on denaturant concentration (Pace *et al.*, 1989).

2.5.3 Determination of dissociation constants

The binding to hydrophobic groups on protein surfaces enhances the fluorescence intensity of ANS. This allows the exploitation of this property to study interactions with the proteins. The displacement of ANS bound to wild type hGSTA1-1 or R15L by GSO_3^- was determined by monitoring the reduction of ANS fluorescence upon addition of GSO_3^-. ANS was at a constant concentration of 200 μM and was displaced via successive aliquot additions of GSO_3^- . GSO_3^- Stock solutions of 3 mM, 1 mM and 0.5 mM were used. The final volume in the cuvette after the successive aliquot addition of GSO_3^- was 521.5 μM, 528 μM and 551.5 μM for the respective stock solutions. ANS was excited at 390 nm. Emission was monitored between 400 and 600 nm with the emission maximum occurring at 475 nm. The experiments were carried out in 20 mM sodium phosphate, 100 mM NaCl, 1 mM EDTA and 0.02 % sodium azide, pH 7. Wild type hGST A1-1 and R15L were at a concentration of 2 μM. The experiments were performed at 20ºC using a Perkin Elmer luminescence spectrometer LS50B. The final volume of ANS added did not exceed 10% of the initial volume. As the monitored molecule was ANS and the ANS concentration was kept constant, there were no corrections for inner filter effect performed. However, the dilution of the sample, as the GSO_3^- concentration increased, was taken into account and accordingly corrected for. The data was analysed via non-linear regression analysis, using SigmaPlot v.8.0.

2.6 Isothermal titration calorimetry

2.6.1 ANS and GSO_3^- binding to R15L

The R15L variant protein purified from a CM-Sepharose column was dialysed against 3 buffer exchanges (20 mM sodium phosphate, 100 mM NaCl, 1 mM EDTA and 0.02% sodium azide, pH 6.5). The dialysis buffer was changed every 6 hours. Dialysis was carried out using dialysis tubing with a molecular mass cut-off of 3500 Da. ANS and GSO_3^- were prepared in dialysate buffer from the final dialysis change. The protein and ligand samples were centrifuged at 12 000xg for 30 minutes at 4°C in order to remove any aggregate matter. The protein concentration was determined as specified in section 2.2.3.

The energetics of R15L·ANS and R15L·GSO_3^- interactions were studied using a VP-ITC Microcalorimeter from MicroCal Incorporated. In a typical experiment, the protein, at monomer concentrations ranging from 69 to 336 μM, for ANS and 164 to 214 μM, for GSO_3^- was loaded into the sample cell of approximately 1.4 ml and ANS or GSO_3^- was loaded into the syringe. The system was allowed to equilibrate and a stable baseline was obtained prior to initiation of the automated titration. A titration consisted of injections ranging in volume from 3 to 10 μl. The concentration of stock ANS ranged from 11.7 mM to 30.3 mM and of GSO_3^- from 10 mM to 12 mM. The appropriate ligand was loaded into the sample cell. The baseline was allowed to restabilise for 3 minutes prior to the subsequent injection. Throughout the titration, the cell was stirred at 300 rpm. The heat change accompanying every injection was displayed as peak and integration of the area underneath the peak using ORIGIN v.5 gave the heat evolved on ANS or GSO_3^- binding to hGST A1-1. The heat of ANS or GSO_3^- dilution was corrected by subtracting the average heat of the last few injections. Data fitting was conducted using ORIGIN v.5. Data were fit to both one-site, two-site and sequential-site fitting models. The best fit was obtained for one-site fitting model. For GSO_3^- the stoichiometry was fixed at 0.7 and for ANS the stoichiometry was fixed at 1. The fitting to this model gives values for ΔH, N and K_a. The other parameters ΔS and ΔG are obtained using equations (2) and (6) (section 1.1.1).

2.6.2 Temperature dependence of thermodynamic parameters

The temperature dependence of the thermodynamic parameters was evaluated in the temperature range 5-25ºC. Experiments were carried out in 20mM sodium phosphate, 100 mM NaCl, 1 mM EDTA and 0.02% sodium azide, pH 6.5. ΔCp was obtained as the slope of the linear plot of ΔH versus temperature in kelvin.

Chapter 3

Results

3.1 Generation, expression, purification and characterisation of R15L hGST A1-1 variant

The replacement of an arginine codon at position 15 with leucine codon (i.e. the generation of the R15L variant) is shown in Figure 7. A suitable clone (Amp selected) was sequenced by Inqaba Biotech ® to confirm the substitution of a AGA codon 15, corresponding to the amino acid Arg15 of hGST A1-1, with a TTA codon encoding for the amino acid Leu. The cDNA nucleotide sequence expressing hGST A1-1 forms part of pKHA1 plasmid (Stenberg *et al.*, 1992). The substitution of the AGA codon with the TTA codon is reflected in panel A of the above-mentioned figure. In panel B, the sequencing results indicate the incorporation of the desired mutation in the parental plasmid cDNA.

Induction studies (with standardised samples) of the *Escherichia coli* BL21 (DE3) cells containing the mutated pKHA1 plasmid (R15L mutation) were done in order to determine optimal over-expression time. The results are shown in Figure 8. These indicated that bacterial cultures grown in the presence of 0.6 mM IPTG produced a protein corresponding to the purified wild type hGST A1-1 marker (Figure 8, Lane 9). Optimal conditions for protein over-expression were achieved using 0.6 mM IPTG for 16 hours (Figure 8, Lane 8).

Solubility of the variant R15L is shown in Figure 9. The markers used are shown in Panel A lane 1.In lane 3 of the 15% SDS-PAGE gel, can be seen the cytosolic content of the *Escherichia coli* BL21 (DE3) cells while whole cell suspension can be seen in lane 4. The electrophoretically pure R15L can be seen in lane 5. The molecular mass of the variant R15L (~24kDa) was estimated from linear regression analysis of a calibration curve (Figure 9, Panel B) for the marker proteins used. Substantial amount of protein is “lost” in the flow-through from a CM-Sepharose cation exchange chromatographic elution (lane 2) as the capacity of the column was exceeded (i.e. the binding sites of the column were saturated and the rest of the protein was carried in the flow-through).

A.

5′-AAT GCA CGG GGC AGA ATG GAG TCC ACC-3′ (wt hGST A1-1)

5′-AAT GCA CGG GGC TTA ATG GAG TCC ACC-3′ (R15L)

B.

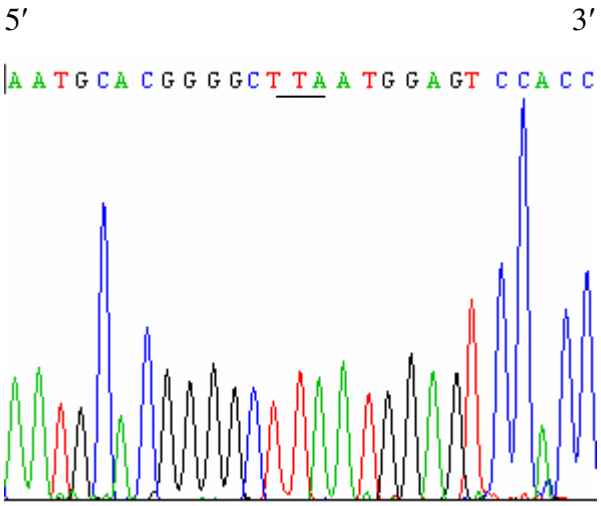


Figure 7. Generation of R15L (A) A portion of the nucleotide sequence of the pKHA1 plasmid DNA encoding wild type hGST A1-1 (Stenberg *et al.*, 1992) showing the position of the Leu15 (TTA codon) in red. The replacement of an arginine codon at position 15 with leucine codon is indicated with an arrow (AGA→TTA). (B) A segment of the nucleotide sequence obtained from DNA sequencing of the R15L mutant pKHA1 plasmid showing the presence of a leucine codon (TTA) at position 15.

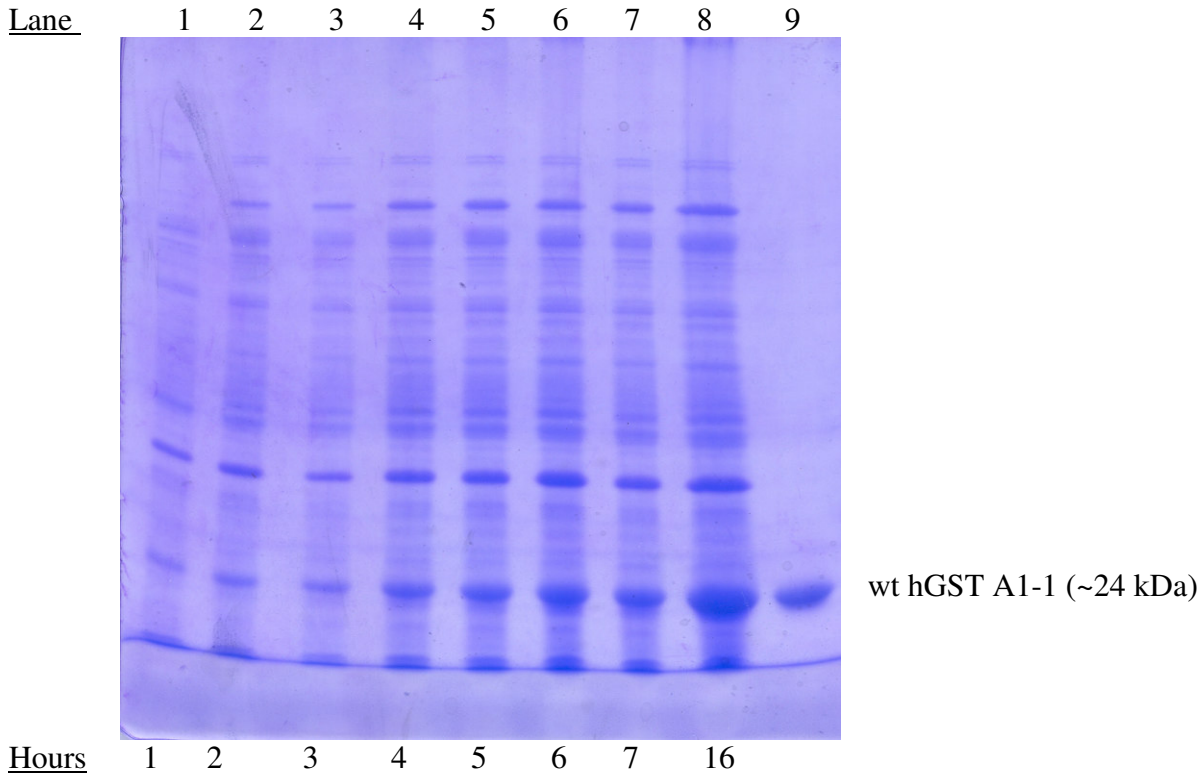
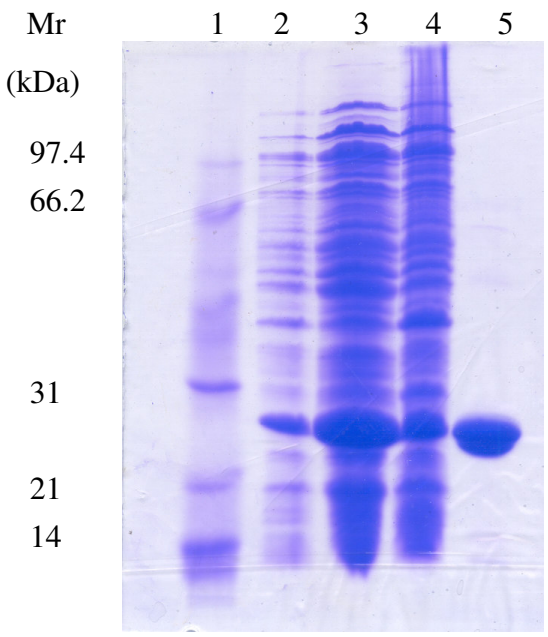


Figure 8. 15% SDS-PAGE separation of *Escherichia coli* BL21 (DE3) proteins from induction studies done with over-expressed R15L variant. R15L over-expression in the bacterial cells was induced with 0.6 mM IPTG. Samples for the SDS-PAGE were taken at various time periods (1-16 Hours (bottom of figure)). Lanes 1-8 (top of figure): 0.6 mM IPTG time course induction studies for the R15L with sampling time intervals shown on the bottom of the gel. Lane 9: Purified wt hGST A1-1 used as marker.

A.



B.

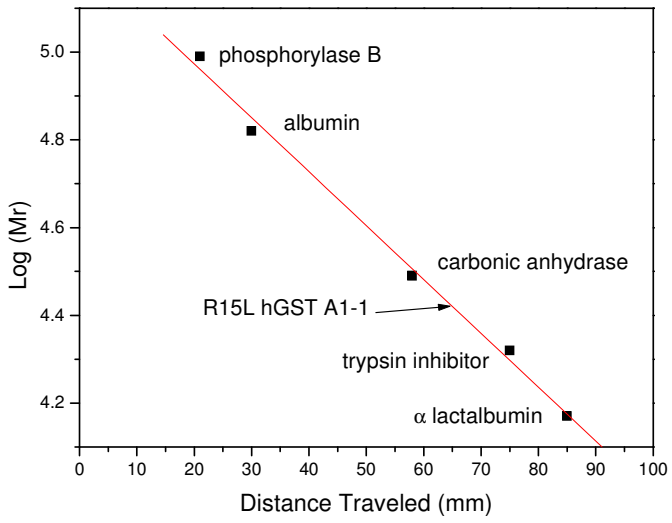


Figure 9. 15% SDS-PAGE of purified R15L and a calibration curve. Panel A: Lane 1: Molecular mass markers (Amersham®). Lane 2: Flow through from CM-Sepharose cation exchange chromatographic elution. Lane 3: Supernatant (cytosolic content) from sonicated and centrifuged *Escherichia coli* BL21 (DE3) containing the mutated pKHA1 (R15L mutation). Lane 4: Whole cell suspension. Lane 5: CM-Sepharose purified R15L. Panel B: Calibration curve of Log (Mr) vs distance traveled (mm) where the values are taken from Panel A Lane1. The R^2 for the fitted line through the points is 0.99 and the molecular mass of the protein (R15L) is determined as 24 kDa.

The far-UV (250-210 nm) circular dichroism spectral characterisation of the wild type and the variant R15L is depicted in Figure 10. Both proteins were at 2 μM concentration, and no significant difference was observed between the two spectra. The two proteins each exhibited troughs at 222 nm and 208 nm, which is typical of proteins predominated by α helices. This is consistent with the crystal structure of hGST A1-1, which reports that the protein is predominantly alpha-helical (Sinning *et al.*, 1993).

Thus, it can be concluded that the substitution of Arg15 with Leu did not create any detectable overall changes in the secondary structural content of the variant protein.

.

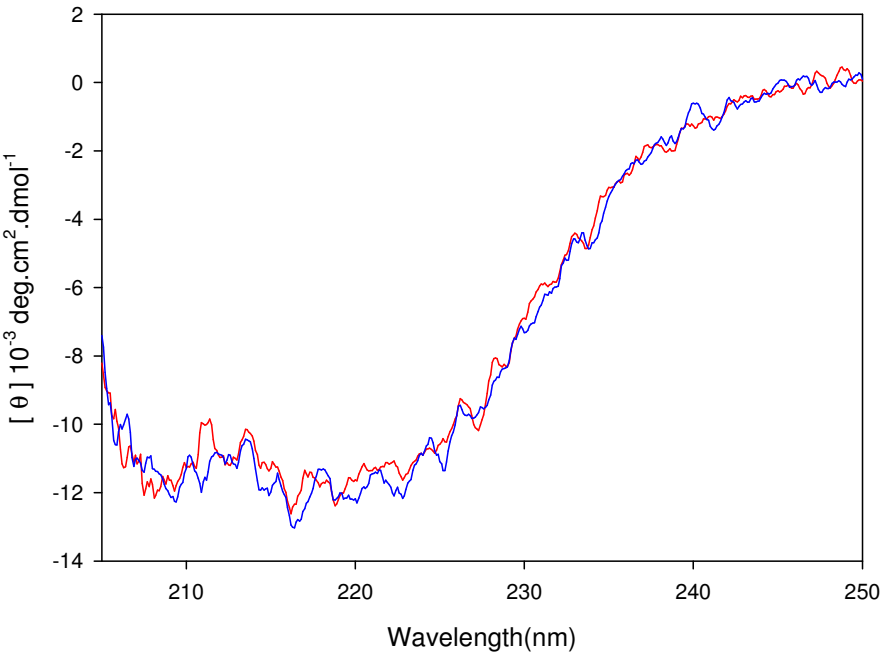


Figure 10. Far-UV circular dichroism spectra characterisation of the wild type hGST A1-1 (---) and the variant R15L (---) proteins in 20 mM sodium phosphate buffer, pH 6.5, containing 1mM EDTA and 0.02% sodium azide. The protein concentration used for both the hGST A1-1 and R15L variant was 2 μM.

3.2 Conformational stability and unfolding of R15L

Urea-induced equilibrium unfolding curves for R15L variant are presented in Figure 11. The unfolding of the proteins was monitored by fluorescence (selectively exciting Trp21 at 295 nm) and via far-UV circular dichroism (CD) (monitored at 222 nm). For comparative purposes included in Panel B, Figure 11 are the urea-induced equilibrium unfolding curves of the wild type protein (Mosebi *et al.*, 2003).

Single sigmoidal curves characterise the unfolding transition of both wt hGST A1-1 and R15L variant, suggestive of a two-state (folded dimer/unfolded monomer) transition. This indicates the absence of any identifiable thermodynamically stable intermediates. It also reflects the nature of the unfolding as a cooperative reaction (Privalov, 1992). Thus, data fitting was performed according to a two-state model, the free energy change in the absence of denaturant ($\Delta G(H_2O)$) and the cooperativity (m-value) of protein unfolding were determined via non-linear regression analysis (Pace, 1986; http://www.wits.ac.za/mcb/bcb/).

It is evident from Figure 11(A) that the unfolding transition regions for R15L when monitored via fluorescence (selectively exciting Trp21 at 295 nm) and via far-UV circular dichroism (CD) (monitored at 222nm) are not superimposable.

Major differences, including free energy change in the absence of denaturant, changes in the unfolding transition mid-points (C_m-value), as well as differences in the slope of the transition regions, are observed for the variant protein relative to the wild-type protein when monitored via Trp21 fluorescence (Table 3). With the exception of the C_m-values, however, no significant differences were observed for the variant R15L relative to the wild-type protein when monitored via far-UV CD (Table 3).

When monitored via Trp21 fluorescence, the unfolding transition for the variant R15L is broad relative to the wild type protein. Further, the variant protein appears less stable (decreased $\Delta G(H_2O)$ value) relative to the wild type protein. However, the unfolding transition midpoint (C_m-value) is at a higher urea concentration relative to the wild type protein (Table 3).

When monitored via far-UV CD, broadening of the unfolding transition is not observed, neither is there a significant decrease in the $\Delta G(H_2O)$ value. However, there is a slight increase in the C_m-value (Table 3).

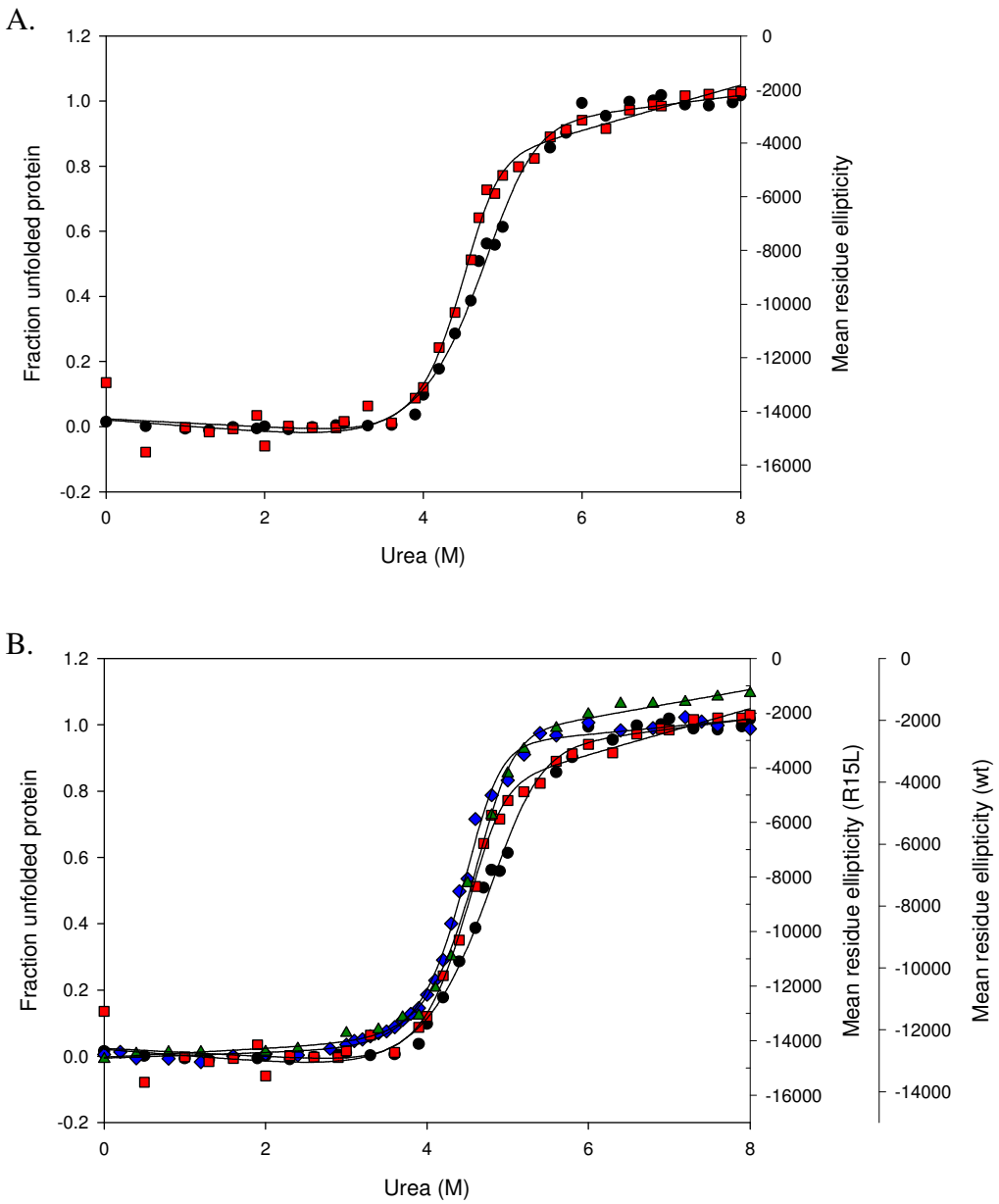


Figure 11. Urea-induced equilibrium unfolding curves for R15L. Panel (A) shows a comparison of R15L unfolding curves monitored via Trp21 fluorescence, converted to fraction unfolded protein (●) and far-UV CD at 222 nm, converted to mean residue ellipticity (■). Panel (B) shows wild type hGST A1-1 unfolding curves (Mosebi *et al.*, 2003) monitored via Trp21 fluorescence, converted to fraction unfolded protein (♦) and far-UV CD at 222 nm, converted to mean residue ellipticity (▲), included for comparative purposes. The variant R15L (2 μM) was in 20 mM sodium phosphate buffer containing 100 mM NaCl, 1 mM EDTA and 0.02% sodium azide, pH 6.5 at 20°C. The fraction unfolded protein was plotted, where it represents the ratio of fluorescence intensity at 355nm (unfolded) to that at 330nm (folded) as an increase in fraction (0-1) of unfolded protein, as a function of increasing urea concentration (0-8M).

Table 3: A comparison of thermodynamic properties of the wild type protein with R15L variant determined from unfolding experiments using fluorescence and circular dichroism as probes. The wild type data was included for comparative purposes (Mosebi *et al.*, 2003)

Parameter	Wild-type	R15L hGST A1-1
Fluorescence		
ΔG (H_2O) (kcal mol^{-1})	22.8 ± 0.98	18.2 ±0.98
m-value (kcal mol^{-1} M^{-1})	3.3 ± 0.22	2.3 ± 0.2
C_m (M)	4.5	4.8
Circular dichroism		
ΔG (H_2O) (kcal mol^{-1})	22.6 ± 1.02	22 ± 1.74
m-value (kcal mol^{-1} M^{-1})	3.2 ± 0.22	3.3 ± 0.38
C_m (M)	4.5	4.6

3.3 Steady state enzyme kinetics

3.3.1 CDNB conjugating activity of R15L

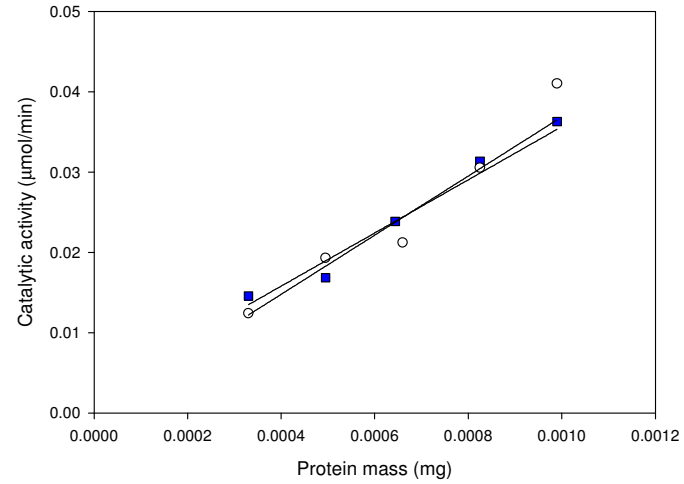
The specific activity of the R15L variant protein was determined using the standard GST/CDNB-conjugation assay (Habig and Jakoby, 1981). In the initial experiments, where final protein concentrations of up to ~ 5 nM were used in each assay, R15L variant protein displayed no catalytic activity. Consequently, substantially higher protein concentrations (> 50 nM) were used to assay for activity of this protein. Furthermore, in an attempt to improve the signal to noise ratio of the linear progress curves observed for this protein, measurements were made at 340 nm for 30 seconds, as opposed to the 60 seconds measured for the hGST A1-1 variant protein. Under these conditions, the measurement of the catalytic activity of the R15L variant protein was made possible.

The average specific activitiy of R15L variant protein was determined to be 1.53 μmol/min/mg from the two repetitions (Figure 12 (B)), and the value for the wild type protein was determined as 34.9 μmol/min/mg (Figure 12 (A)). Thus, the R15L variant protein displayed 4.4 % activity relative to the determined wild-type values.

3.3.2 The effect of BSP on CDNB conjugating activity of R15L

To assess the effect of BSP on hGST A1-1 and R15L CDNB-conjugating activity, standard assays were performed in the presence of variable concentrations of BSP. IC_{50} – values were determined (IC_{50}=32μM for wild type and IC_{50}= 62μM for R15L) from the non-linear regression analysis of the data (Figure 13). It has been proposed that the wild type hGST A1-1 possesses two types of binding sites: a high affinity and a low affinity set of binding sites (Kolobe *et al.*, 2004). The former accommodates one molecule of BSP, whereas the latter accommodates 3 molecules of BSP (Kolobe *et al.*, 2004). BSP binding at the high affinity site has a K_d of 0.12 μM (Kolobe *et al.*, 2004) and from Figure 13 Panel A it can be observed that the binding of BSP does not affect the enzymatic activity of hGST A1-1 (Kolobe *et al.*, 2004).

A.



B.

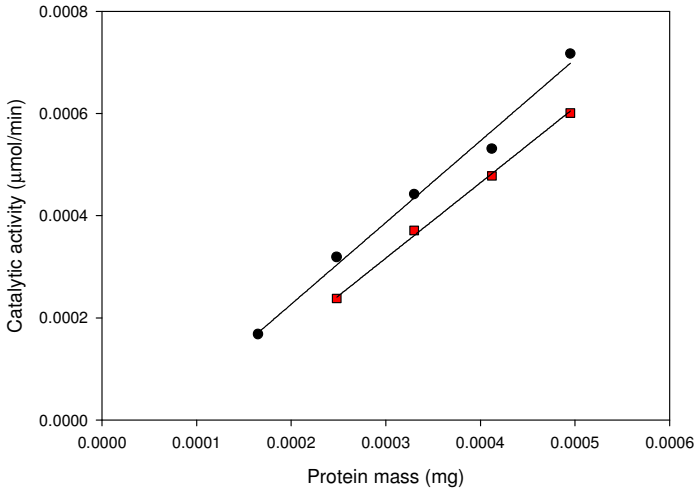


Figure 12. Determination of the specific activity of the (A) wild-type and (B) R15L proteins. The solid lines represent the linear fit to the experimental data. Two repetitions of the assay are shown ((○) and (■) for wild type and (●) and (■)) for R15L). The specific activity of each protein was determined from the slope of the graph using SigmaPlot v8.0, with a linear regression analysis (R^2(○) = 0.95 and R^2(■)= 0.95 hGST A1-1 data; R^2(●) = 0.99 and R^2(■)= 0.99 for R15L data).

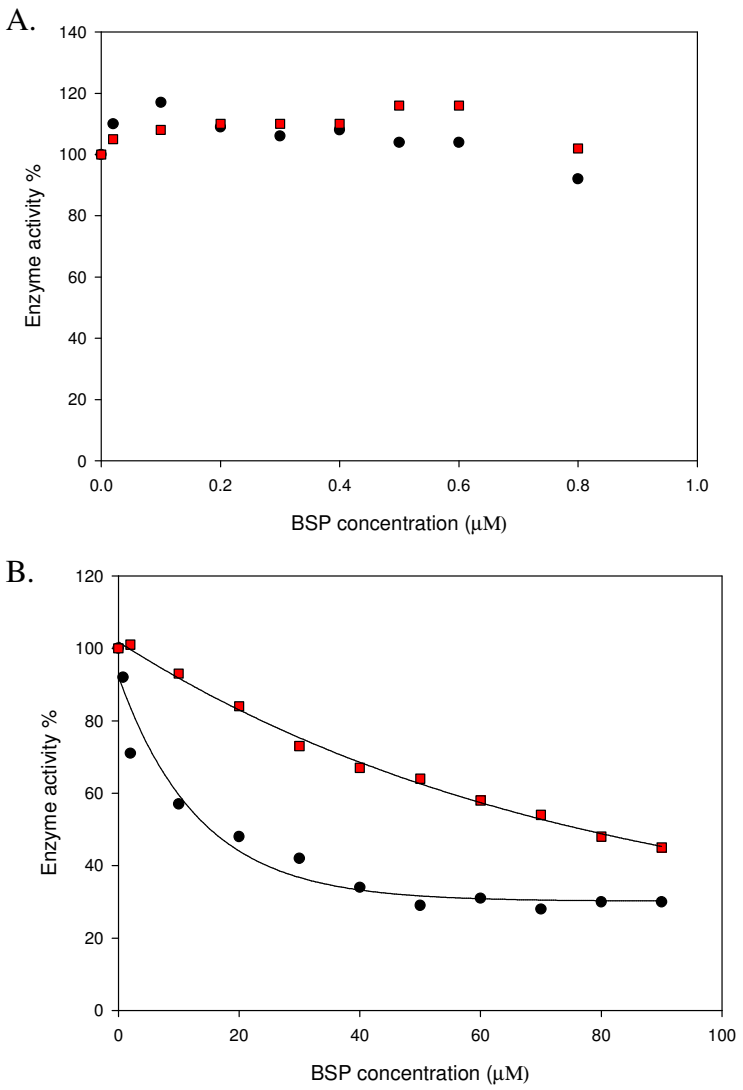


Figure 13. Inhibition of wild type and R15L hGST A1-1 CDNB-conjugating activity by BSP. Panel A depicts the CDNB-conjugating activity in the presence of low BSP concentrations (0-1μM) for wild type (●) and variant R15L (■) hGST A1-1. Panel B represents the same conjugating activity in high BSP concentrations (0-90μM) for wild type (●) and variant R15L (■) hGST A1-1. The assay was performed in 20 mM phosphate buffer, containing 100 mM NaCl, 1 mM EDTA and 0.02% sodium azide, pH 6.5.

However, at higher concentrations of BSP the enzyme activity of hGST A1-1 is inhibited. The same argument applies for the variant R15L. BSP binding at the high affinity site (proposed for the wild type) has no effect on the enzymatic activity of R15L. However, the enzymatic activity is inhibited for the low affinity site (proposed for the wild type).

3.4 Displacement studies

3.4.1 Spectral properties of hGST A1-1 and R15L bound ANS

The spectral characterisation of the wt hGST A1-1 (2 μM) and R15L variant (2 μM) was carried out by selectively exciting Trp21 at 295 nm. Figure 14 shows the emission spectra obtained for the wild-type and variant hGST A1-1 proteins in the absence and presence of 200 μM ANS final concentration. The chemical structure of ANS is depicted in Figure 15. The emission maxima of the wt hGST A1-1 and R15L proteins in the absence of ANS, was found to be at 330 nm, consistent with the burial of the Trp21 residue in the native state of the protein (Wallace *et al.*, 1998a; Wallace *et al.*, 1998b). Following addition of ANS, the emission maxima were found at 475nm for both wt and R15L proteins, which is characteristic of ANS emission when bound to hydrophobic surface areas on protein.

The spectra of wt hGST A1-1 and R15L in the absence of ANS are nearly superimposable (Figure 14). A slight decrease in fluorescence intensity (approximately 4 %) was observed in the emission spectrum of the R15L variant when compared to that of wt hGST A1-1. This could be accounted for as an experimental error. Thus, it can be concluded that no gross structural changes occurred due to the Arg15 to Leu substitution. Moreover, this similarity is indicative of the tertiary structure of the R15L variant protein being equivalent to that of the wild-type hGST A1-1 protein.

The spectra of hGST A1-1 in the absence and presence of ANS showed a slight increase of the emission maximum in the presence of ANS (Figure 14). As the increase was 4%, it can be argued as above that there was an experimental error.

When emission maxima of wt hGST A1-1 and R15L are compared in the presence of ANS it is observed that there is a substantial (37%) drop in intensity, indicative of reduced number of bound ANS molecules to R15L. Further, there was also a substantial

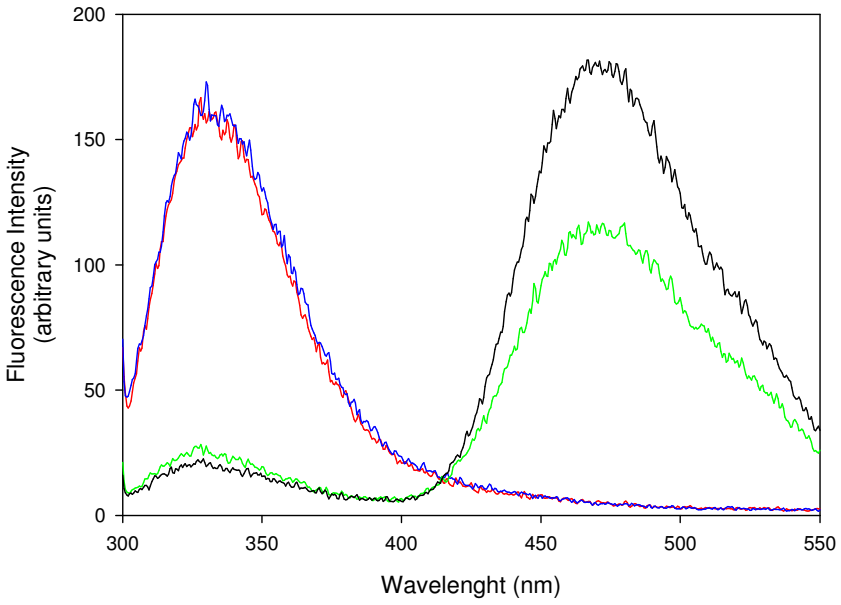


Figure 14. Fluorescence spectral characterisation of wild type (blue and black) and R15L (red and green) in 20 mM sodium phosphate buffer, pH 6.5 containing 100 mM sodium chloride, 1 mM EDTA and 0.02% sodium azide. The lone tryptophan 21 was selectively excited at 295 nm and the wavelength emission monitored. The wavelength emission maximum for the native proteins is at 330 nm for native proteins (blue and red). The wavelength emission maximum is at 475 nm for the energy transfer from the excited tryptophan 21 to the ANS bound to the proteins (black and green).

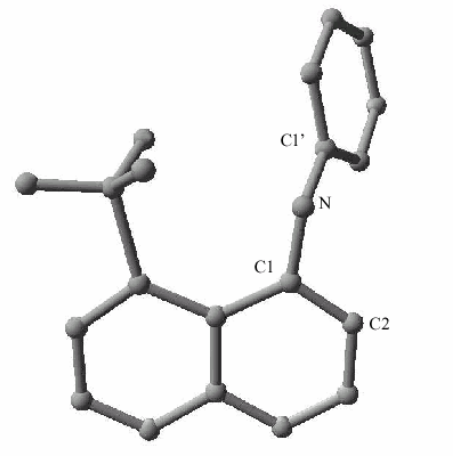


Figure 15. The structure of the organic anionic dye ANS. Figure taken from Sayed *et al.,* 2002.

decrease in the emission maximum intensity (31%) for R15L in the presence of ANS relative to the data in the absence of ANS (Figure 14).

3.4.2 Glutathione sulphonate displacement of ANS

In order to asses the binding affinity of GSO_3^- (Figure 16) for the wild type hGST A1-1 and R15L variant, a displacement of the amphipathic dye ANS (Figure 15) with GSO_3^- was performed. The displacement of ANS with GSO_3^- was monitored via a change in the fluorescence signal of the excited ANS bound to either the wild type or R15L protein. The displacement process, monitored via a change in fluorescence intensity, was analysed via non-linear regression analysis and the dissociation constant of glutathione sulphonate was determined for the wild type (K_d = 46.6μM) but not for R15L as no displacement of ANS with GSO_3^- was evident for the variant protein (Figure 17).

3.5 Isothermal titration calorimetry

The calorimetric profiles of the titration of R15L with ANS (Figure 18) or GSO_3^- (Figure 19) indicate that the complex formation has an exothermic heat signal. Panel A, in both figures, represents the raw data changes in real time. As the titration injection number and volume increases, R15L variant binding site(s) become(s saturated with ANS or GSO_3^-. The heat signal at the end of the titration becomes uniform, indicative of heats of dilution. Panel B represents the integrated heats of the peaks in Panel A, corrected for heats of dilution. The trace in Panel B is hyperbolic. In other words, as the injected volume of ligand into the cell increases the slope of the curve changes until it becomes zero and the curve is parallel to the x-axis (molar ratio [ANS/R15L] or [GSO_3^-/R15L]). The tangent to the curve also becomes zero, indicative of the saturated state of the binding reaction between R15L and ANS or GSO_3^-.

R15L binding curves, for both ANS and GSO_3^-, fit well to a one set of sites binding model describing one binding site per variant subunit. The binding of one ANS molecule per site was consistent with the wild type data (Sayed *et al.*, 2002) and so was the binding of GSO_3^- (Sayed, unpublished data). The stoichiometry (N) was fixed upon data analysis. This is necessary at low c-values (c-value between 1 and 0.01) as the curve fitting

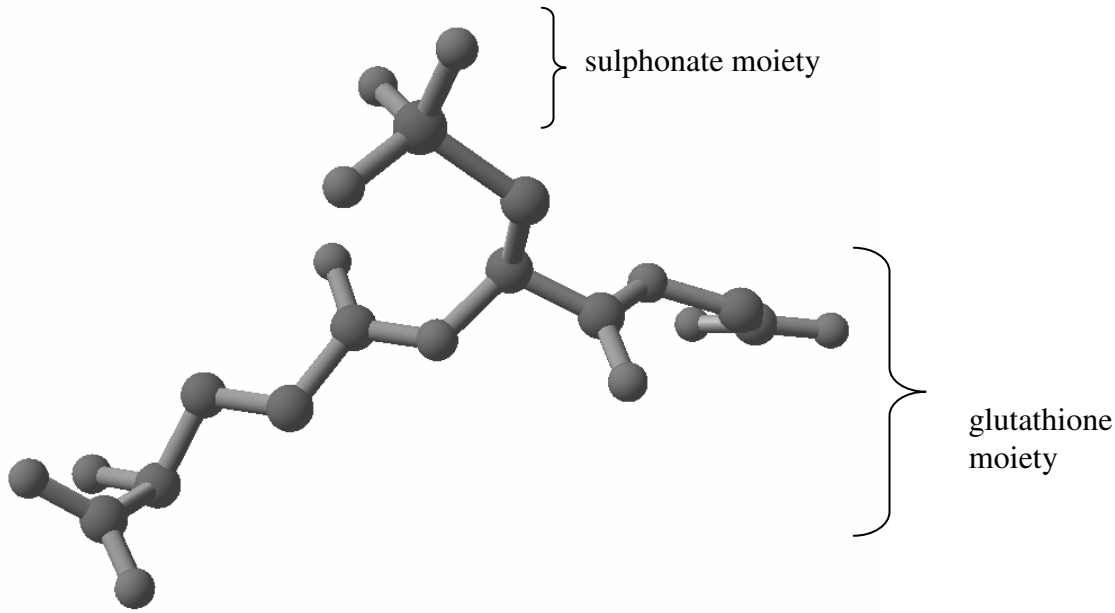


Figure 16. The structure of the GST ligand glutathione sulphonate (pdb code 1ev4 Adman *et al.,* 2001). The figure was generated using Swiss-Pdb Viewer (Guex and Peitsch, 1997).

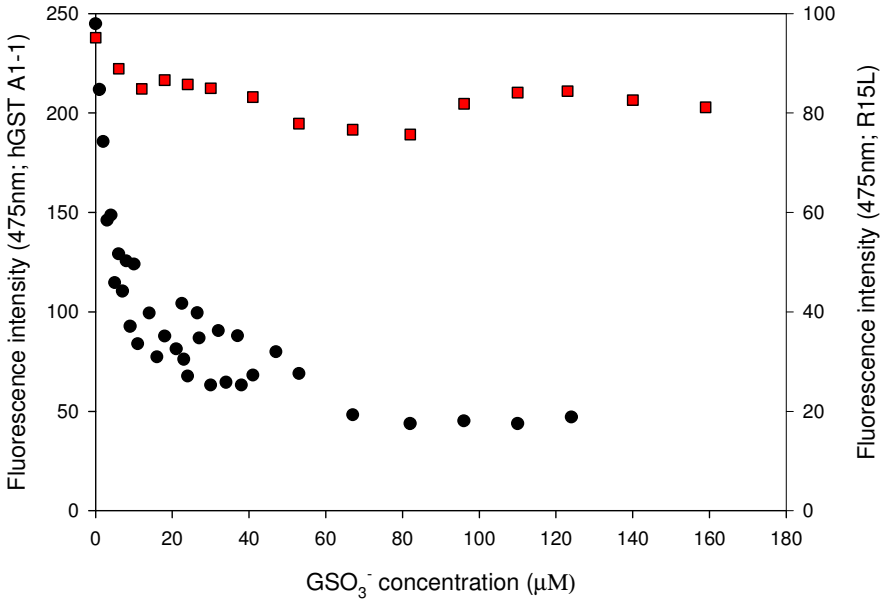


Figure 17. Displacement of ANS bound to wt hGST A1-1(●) and R15L(■) by GSO_3^-. The displacement of ANS (200 µM final concentration) bound to wt hGST A1-1 (2 µM) or R15L (2 µM) was done by titrating increasing concentrations of GSO_3^- (0-160 µM). ANS was selectively excited at 390 nm and the emission florescence intensity monitored at 475 nm. The buffer used was 20 mM phosphate, 1 mM EDTA, 100 mM sodium chloride and 0.02% sodium azide at pH 6.5.

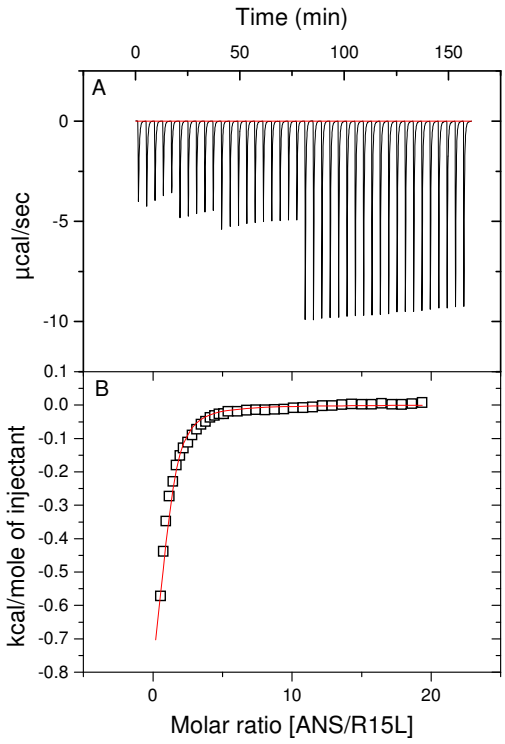


Figure 18. A calorimetric profile for the titration of R15L hGST A1-1 with ANS. The experiment was performed in 20 mM sodium phosphate buffer containing 100 mM NaCl, 1 mM EDTA and 0.02% sodium azide, pH 6.5 at 5°C. Panel A shows the raw data generated by titration of 336 µM protein monomer with injections of 30.3 mM ANS stock. Panel B shows the integrated heats for the above peaks (corrected for heats of dilution) plotted against molar ratio of ANS to protein monomer. The continuous line represents the non-linear least-squares fitting of the experimental data to the one-site binding model. The data was analysed with ORIGIN v.5.0.

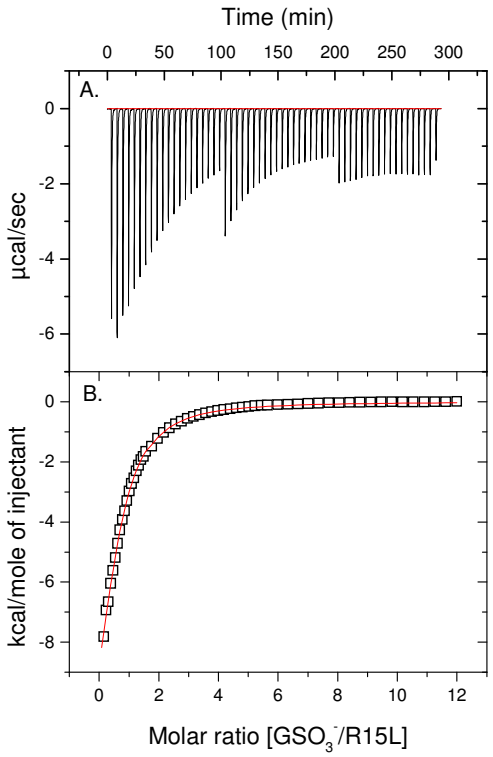


Figure 19 A calorimetric profile for the titration of R15L hGST A1-1 with GSO_3^-. The experiment was performed in 20mM sodium phosphate buffer containing 100 mM NaCl, 1 mM EDTA and 0.02 % sodium azide, pH 6.5 at 20°C. Panel A shows the raw data generated by titration of 214 µM protein monomer with injections of 12 mM GSO_3^- stock. Panel B shows the integrated heats for the above peaks (corrected for heats of dilution) plotted against molar ratio of GSO_3^- to protein monomer. The continuous red line represents the non-linear least-squares fitting of the experimental data to the one-site binding model. The data was analysed with ORIGIN v.5.0.

becomes over parameterised and may not converge unless N is kept constant (Turnbull and Daranas, 2003).

Thermodynamic parameters obtained from data fiting for R15L·ANS complex formation for a temperature range (5-25°C) are presented in Table 4 whereas Table 5 represents the data for R15L·GSO_3^- complex formation at the indicated temperature range. The dissociation constants (K_d) over the specified temperature range, for the binding of ANS by R15L, are higher in magnitude (2 to 5 times for the corresponding temperatures) relative to the dissociation constants for GSO_3^- binding, thus indicating that the ANS binding is weaker relative to the GSO_3^- binding to R15L. The ANS free energy of binding over the specified temperature range is lower than the free energy for the binding of GSO_3^- by about 2.5-5kJ/mol, indicating less stable R15L·ANS complex relative to the R15L·GSO_3^- complex.

Temperature dependence of thermodynamic parameters including change in enthalpy (ΔH), change in entropy (ΔS) and change in free energy (ΔG) are shown in Figure 20 for the binding of ANS and in Figure 21 for the binding of GSO_3^-. For both ANS and GSO_3^- binding ΔH, $T\Delta S$ parameters exhibited strong dependency on temperature, with linear regression coefficients (R^2) in the range of 0.86 to 0.95. The free energy of ANS binding also exhibited a strong dependency on temperature, with R^2 of 0.88. However, for the binding of GSO_3^-, very weak dependency on temperature was shown by $\Delta G°$ as the R^2 value was 0.31, indicating tendency towards a horizontal regression line.

The change of enthalpy over the specified temperature range (Table 4 and Table 5) for both R15L·ANS and R15L·GSO_3^- complex formation is exothermic. The binding of ANS has a range of enthalpy values which defines a steeper increase over the measured temperature range relative to the binding of GSO_3^- (Figure 20 and Figure 21).

The change in entropy over the experimental range for the binding of GSO_3^- is unfavourable and becomes more unfavourable with increasing temperature. However, for the binding of ANS the change in entropy is favourable over the entire temperature range of 5 to 25°C. Thus, the differences in ΔH and ΔS for the R15L·ANS and R15L·GSO_3^- complex formation reflect differences in the types of interactions due to the differences in the nature of the two ligands used.

Table 4. Thermodynamic parameters for the binding of ANS to R15L hGST A1-1 at various temperatures. The stoichiometry was fixed.

T (°C)	N	K_d (μM)	ΔH_{obs} (kJ/mol)	TΔS (kJ/mol)	ΔG (kJ/mol)
5	1	118	-4.1	16.8	-20.9
10	1	143	-13	7.8	-20.8
20	1	189	-17.8	3.1	-20.9
25	1	215	-18.6	2.3	-20.9

Table 5. Thermodynamic parameters for the binding of GSO_3^- to R15L hGST A1-1 at various temperatures. The values are taken as average of two experiments and the stoichiometry was fixed.

T (°C)	*N*	K_d (μM)	ΔH_{obs} (kJ/mol)	TΔS (kJ/mol)	ΔG (kJ/mol)
5	0.7	25	-45.9	-21.0	-24.9
10	0.7	35	-49.2	-24.9	-24.3
15	0.7	81	-49.2	-26.2	-23.0
20	0.7	75	-53.7	-30.5	-23.3
25	0.7	118	-59.1	-36.6	-22.5

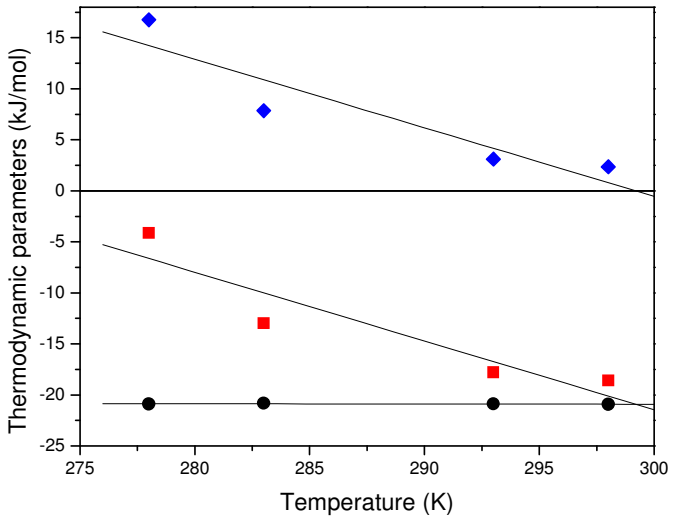


Figure 20. Temperature dependence of the thermodynamic parameters for the binding of ANS in the presence of 100 mM NaCl. The experiments were performed in 20mM sodium phosphate, 1 mM EDTA, 0.02% sodium azide, pH 6.5. The solid lines represent linear fits to the experimental data. ΔH(■), R^2=0.86; $T\Delta S$(♦), R^2=0.86; ΔG(●), R^2=0.31. Heat capacity changes associated with the binding were determined from the slope of the plot of ΔH_{obs} versus temperature.

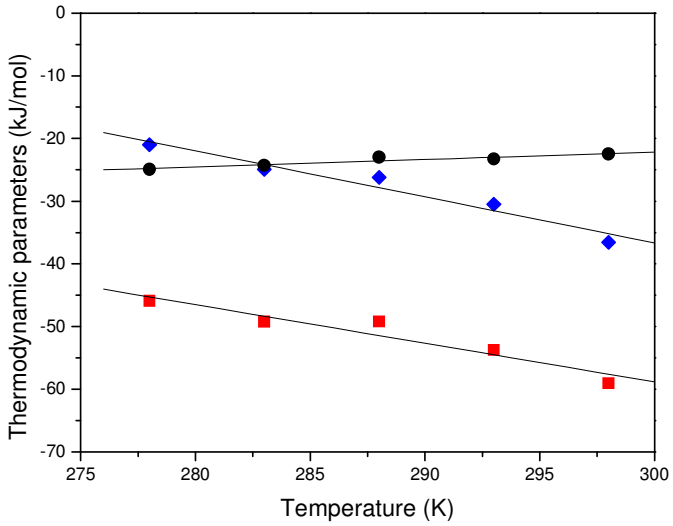


Figure 21. Temperature dependence of the thermodynamic parameters for the binding of GSO_3^- in the presence of 100mM NaCl. The experiments were performed in 20 mM sodium phosphate, 1 mM EDTA, 0.02% sodium azide, pH 6.5. The solid lines represent linear fits to the experimental data. ΔH(■), R^2=0.91; $T\Delta S$(♦), R^2=0.95; ΔG(●), R^2=0.88. Heat capacity changes associated with the binding were determined from the slope of the plot of ΔH_{obs} versus temperature.

Chapter 4

Discussion and Conclusion

4.1 Conformational stability

The equilibrium unfolding of R15L (Figure 11(A)) follows a monophasic sigmoidal unfolding transition. Sigmoidal unfolding transitions, which are characteristic of the unfolding process, reflect the nature of the unfolding event as a cooperative reaction (Privalov, 1992) . The cooperative process is well-known for simple dynamic equilibria and is characteristic of a variety of proteins (Schmid, 1992) including the GST family (Dirr and Reinemer, 1991; Erhardt and Dirr, 1995; Kaplan *et al.*, 1997; Wallace *et al.*, 1998b). The monophasic sigmoidal unfolding transition for R15L suggests a two state unfolding transition from the native dimer (N_2) to the unfolded monomer (U).The absence of a thermodynamically stable monomeric or dimeric intermediate(s) for the R15L unfolding suggests that each monomer cannot be separated into distinct folding units thus following the same trend as the wild type protein hGST A1-1 (Wallace *et al.*, 1998b).

Compared with unfolding data for wild type protein, the R15L does not display significant decrease in stability, when monitored via far-UV CD (Table 3). Neither is the *m*-value significantly affected. However, the *m*-value decreases for R15L equilibrium unfolding when monitored via Trp21 fluorescence (Table 3).The decrease in the *m*-value indicates that the variant is denatured over a broader range of urea concentrations. There are three possible reasons for the decrease in the *m*-value: (i) a difference in the exposed surface area of the native and /or unfolded state; (ii) a situation whereby an intermediate becomes significantly populated and the R15L variant no longer displays equilibrium two-state unfolding behaviour; or (iii) changes in the interactions of the denaturant with the molecules in the denatured state (Wallace *et al.*, 1998a and references therein). The applicability of (i) for R15L is low as it would be reflected in coincidence of the unfolding transitions for the variant monitored via far-UV CD and fluorescence (Figure 11 (A)), which is not the case. Also, the possibility of (iii) being applicable is very low, since urea and guanidinium chloride induce complete unfolding GSTs and yield similar values for $\Delta G(H_2O)$ for unfolding (Dirr and Reinemer, 1991), suggesting that there are no

specific binding sites for these denaturants in either the folded or the unfolded protein. Thus, the broader unfolding transition and decreased *m*-value are most probably due to the accumulation at equilibrium of an unfolding intermediate of the R15L variant. Thus, the equilibrium properties of the unfolding reaction are no longer two-state.

Despite the fact that native dimer (N_2) and unfolded monomer (U) are the only states observed for hGST A1-1 equilibrium unfolding studies, unfolding kinetic studies done for hGST A1-1 suggest a sequential three-state unfolding pathway:

$$N_2 \rightarrow N_2^* \rightarrow 2U$$

where N_2^* represents transient intermediate species undergone structural changes at the interdomain interface near Trp21 and the result of the destabilisation/unfolding of helix9 (Wallace *et al.*, 2000). The state N_2^*, appear to be negligibly populated at equilibrium for wt hGST A1-1 (Wallace *et al.*, 1998b). The fast kinetic unfolding phase is represented by $N_2 \rightarrow N_2^*$ transition, whereas the slow kinetic unfolding phase is represented $N_2^* \rightarrow$ 2U. The origin of the fast unfolding phase was proposed to be partial dissociation of domain I from domain II at or near Trp21. The indole side chain of Trp21 protrudes from domain I into domain II. The slow unfolding phase represents the complete dissociation and unfolding of N_2^* into two unfolded monomers (Wallace *et al.*, 1998b). The engineering of the R15L variant results in disruption of Arg15-Glu104 salt link, which is found at the interdomain interface. Thus, it is plausible that the N_2^* species become significantly more populated at equilibrium for the R15L variant unfolding. However, further unfolding kinetic studies are necessary in order to confirm the plausibility of the proposal.

A decrease in the *m*-value and increase in the mid-point of the unfolding transition has previously been observed for the unfolding of pGST P1-1 in the presence of glutathione sulphonate and *S*-hexyl-glutathione (Erhardt and Dirr, 1996). The conclusion in this case was that the two-state fit was no longer applicable and the transition state(s) was stabilised against urea in the presence of these ligands. The reduced cooperativity of unfolding also indicated that there may be a change in the protein's unfolding pathway (Erhardt and Dirr, 1996).

Based on the structural and equilibrium unfolding data for the R15L mutant it can be concluded that the transient state, only detectable by Trp21, is stabilised against urea. Thus, the unfolding pathway of the R15L variant is altered.

4.2 Isothermal titration calorimetry

To date there is no experimental structure of ANS (Figure 15) complexed to hGST A1-1. However, molecular docking and ligand-displacement studies indicate placement of the ligand in the H-site of hGST A1-1 (Dirr *et al.*, 2005). The molecular docking performed assumed that the conformation of the protein C-terminus in the hGST A1-1·ANS complex is the same as observed for other ligands bound to the same protein. The predicted binding of ANS by the docking software is at the H-site of hGST A1-1. However, the binding modes of the molecule differ slightly in the presence and absence of GSH (Dirr *et al.*, 2005).

The nonpolar H-site is occupied by the hydrophobic anilino and naphthyl rings of ANS, which are within van der Waals distance of Leu107, Leu108, Val111, Met208, Leu213, Ala216, Phe220 and Phe222. The negatively charged sulphonate group of ANS is located at the interface between the G-site and the H-site and is within the van der Waals distance of Tyr9, Phe10, Arg15 and Val55 (Dirr *et al.*, 2005). These amino acid residues have been found within van der Waals distance of various other ligands bound at the H-site of hGST A1-1 (Cameron *et al.*, 1995; Le Trong *et al.*, 2002; Sinning *et al.*, 1993). The predominant hydrophobicity of the binding site (H-site) accommodating the anilino and naphthalene rings correlates with the binding sites for ANS found in other proteins (Lartigue *et al.*, 2003; Ory and Banaszak, 1999; Schonbrunn *et al.*, 2000). However, the determinant of the stoichiometry of binding has been suggested to be the sulphonate group when an ion pair is formed with a corresponding lysine, histidine or arginine residue (Matulis and Lovrien, 1998). And in the case of hGST A1-1 there is an arginine residue (Arg15) which would accommodate the formation of such an ion pair.

Arg15 is also in hydrogen bonding distance from the glutathione moiety of glutathione sulphonate, which is accommodated by both the G- and H- sites of GST A1-1 (Adman *et al.*, 2001; Cameron *et al.*, 1995; Sinning *et al.*, 1993). The glutathione moiety is also in hydrogen bonding distance of Tyr9, Arg45, Gln53, Gln54, Val55, Pro56, Gln67, Thr68

from the same subunit and Asp101 and Arg131 from the neighbouring subunit. Of these amino acids, with the exception of Pro56, Gln53 and Gln54, all form hydrogen bonds and/or salt links, positioning the glutathione moiety in the G-site binding pocket and the conjugating partner in the H-site binding pocket (pdb code 1guh; Sinning *et al*., 1993). These amino acids are characteristic for the binding of the glutathione moiety regardless of the presence or nature of a conjugating partner (Sinning *et al.*, 1993).

An interesting observation was that no binding of ANS could be detected when GSO_3^- was present at the active site. The binding mode, at the G-site, of GSO_3^- and GSH is the same; however, the negatively charged sulphonate group of GSO_3^-occupies a similar position to that of ANS bound to the H-site (Dirr *et al.*, 2005). ANS has also been shown to be strongly displaced by ligands that bind H-site for both wt hGST A1-1 and the D209G variant (Dirr *et al.*, 2005). The explanation given for the lack of displacement of ANS by GSO_3^- is that both of them compete for the overlapping binding sites of their sulphonate groups. On the other hand, GSH does not displace ANS as there is no competition for a binding space and both ligands are accommodated at the active site (Dirr *et al.*, 2005). For the R15L variant, ANS is not displaced by GSO_3^- (Figure 17) and it is plausible that the active site of the variant accommodates both ligands simultaneously. Due to the substitution of Arg15 with Leu, the amino acid side chain length is reduced, thus, possibly allowing the accommodation of both ANS and GSO_3^- at the active site of R15L. Further, in ITC experiments, the affinity of ANS for R15L is shown to be lower at 20°C, than the affinity of GSO_3^- for R15L (Tables 4 and Table 5).

The affinity of R15L (Table 6) for ANS or GSO_3^- is significantly affected by the substitution of Arg15 with Leu when compared to the wild type protein (Sayed *et al.*, 2002). The reduction of affinity for ANS is about four-fold relative to the wild type, whereas for GSO_3^- is about seventy-fold, thus indicating that Arg15 plays much more significant role in binding glutathione conjugates than solely H-site ligands with low affinity such as ANS. The reduction of the R15L variant affinity for GSO_3^- is consistent with previous findings regarding the reduction of the activity of the variant as well as the importance of Arg15 in the binding of glutathione conjugates (Adman *et al.*, 2001; Bjornestedt *et al.*, 1995; Sinning *et al.*, 1993). Despite the massive reduction in affinity

Table 6. Dissociation constants of wild type hGST A1-1 and variant proteins for ANS and GSO_3^-.

Protein	ANS (K_d (μM); 25°C)	GSO_3^- (K_d (μM); 25°C)
wt hGST A1-1	65 (Sayed *et al.*, 2002)	1.7 (Sayed, unpublished results)
R15L	215	118
ΔF222	105 (Sayed *et al.*, 2002)	22 (Dobreva, unpublished results)
I219A	47 (Mosebi *et al.*, 2003)	N.D.*
D209G	52 (Dirr *et al.*, 2005)	N.D.

* N.D. Not determined.

for the binding of GSO_3^- by R15L, the ligand still binds tighter than ANS (Table 6). The reduction of affinity of R15L for ANS or GSO_3^- is thus by far the lowest seen relative to other variants of hGST A1-1 (Table 6). GSO_3^- binds less tightly to R15L than to the ΔF222-deletion variant (Dobreva, unpublished results). ANS binds less tightly to R15L than to the I219A variant (Mosebi *et al.*, 2003), the D209G variant (Dirr *et al.*, 2005) and the ΔF222-deletion variant (Sayed *et al.*, 2002), indicating the significance of this residue in the binding of H-site ligands.

The complex formation across the investigated range of temperatures (5°-25°C) was characterised by constant free energy Table 4 and Table 5. This is due to entropy-enthalpy compensation (Dunitz, 1995; Lumry and Rajender, 1970) characteristic of the R15L·ANS and R15L·GSO_3^- complex formation. Entropy-enthalpy compensation is also characteristic of the free energy of the wild type, ΔF222 variants complexation of ANS or GSO_3^- (Sayed *et al*., 2002; Dobreva, unpublished results), and of the free energy of the I219A and the D209G variants complexation of ANS (Dirr *et al.*, 2005; Mosebi *et al.*, 2003). The free energy of R15L·GSO_3^- complex formation over the experimental range (5°-25°C) is defined by negative enthalpy change (ΔH_{obs}) and a negative entropy change ($T\Delta S_{obs}$). However, the trend of the R15L·ANS complex formation is different. It is characterised by negative enthalpy change (same trend as R15L·GSO_3^- complex formation) and a positive entropy change. Thus, the free energy of complex formation is composed of enthalpic and entropic contributions (see equation (6)). However, to put it into context of the hGST A1-1·X complex formation, where X is a bound substrate or non substrate molecule at the active site, the enthalpic and entropic contributions to the free energy term can be decomposed further. The enthatlpic contributions arise from interactions formed at the binding interface (ΔH_{int}), interactions associated with the folding and localisation α9 helix (ΔH_{loc}), and interactions associated with desolvation and solvation events (ΔH_{solv}). The entropic contributions arise from the conformational constraint of the ligand (substrate or nonsubstrate), C-terminal region and the protein side chains involved in binding upon complexation (ΔS_{conf}). Additional contributions to the entropic term is the release of ordered water molecules into bulk solvent (i.e., desolvation of ligand, protein active site and C-terminal region) or ordering of water molecules during the binding and localisation events (ΔS_{solv}) (Kuhnert *et al.*, 2005).

The enthalpic contributions for the R15L·ANS complex formation come from the predominantly nonpolar nature of ANS and the predominantly hydrophobic site which accommodates it, i.e., the proposed binding at the H-site of hGST A1-1 (Dirr *et al.*, 2005; Sayed *et al.*, 2002). Whereas the enthalpic contributions for the R15L·GSO_3^- complex formation come from the accommodation of the glutathione sulphonate in both the G- and H- sites of GST A1-1 (Adman *et al.*, 2001; Cameron *et al.*, 1995; Sinning *et al.*, 1993). The enthalpic contribution of the localisation of the C-terminal region will be a commonality to both R15L·ANS and R15L·GSO_3^-complex formation, however, due to the different binding regions of the ligands, as well as their structure, the extent of the localisation may differ.

The amphipathic nature of ANS predetermines both hydrophobic interactions involving the aniline and naphthalene rings and polar interactions involving the sulphonate groups. The bulky hydrophobic anilino and naphthalene rings would be shielded from the polar solvent upon binding, bearing favourable entropic contributions due to the release of previously structured water molecules around them. However, as previously suggested by Matulis and Lovrien (1998) the determinant of stoichiometry would be an ion-pair formation involving the sulphonate group of ANS. In the hGST A1-1, a residue found in the 4 Å radius of the docked ANS sulphonate group, namely Arg15 plays an important role in the formation of an ion pair via its guanidino group. The location of the guanidino group of the residue is in the interface between the H- and G- sites of hGST A1-1. The desolvation of the sulphonate group of ANS is enthalpically unfavourable when it is buried in the predominantly hydrophobic H-site of hGST A1-1. The electrostatic interactions formed between the sulphonate group of ANS and Arg15 would, in part, compensate for this unfavourable enthalpy of desolvation by their large exothermic contributions to enthalpy (Matulis and Lovrien, 1998). These electrostatic interactions would be enhanced due to the lower dielectric environment (relative to the bulk solvent) at the predominantly hydrophobic H-site. Such electrostatic interactions between the guanidino group of Arg and the sulphonate group of ANS are demonstrated for other protein-ANS complexes (Lartigue *et al.*, 2003; Ory and Banaszak, 1999; Schonbrunn *et al.*, 2000). I-FABP, for example, is a single domain protein with beta-barrel motif in which cavity the ligand is contained. Despite the fact that the cavity is highly hydrated,

there is only one charge in the pocket likely to electrostatically attract and ionically pair with fatty acid carboxylate (natural ligand), namely Arg106 (Kirk *et al.*, 1996). When this Arg106 is replaced by glutamate, the affinity of I-FABP is reduced by a factor of 20 for oleic acid (Jakoby *et al.*, 1993). It has also been shown that bound fatty acid is displaced by ANS and vice versa, and the proposed mechanism of binding ANS is the initial attraction of the sulphonate moiety to the site ("sensing" the buried Arg106) followed by the aryl rings finding their equilibrium relative twist (Kirk *et al.*, 1996). From experimental structures of ALBP, MurA and PBPs it was observed that there is an Arg residue in the vicinity of the protein bound ANS, namely Arg126 for ALBP (Ory and Banaszak, 1999), Arg91 for MurA (Schonbrunn *et al.*, 2000) and Arg33 for PBPs (Lartigue *et al.*, 2003).

On the other hand, GSO_3^-, which is accommodated at the G-site and H-site of GST A1-1, has a more polar nature than ANS. As described above, numerous residues hydrogen bond or salt-link with the tripeptide of GSO_3^-, thus an enthalpically unfavourable desolvation of glutathione will be opposed by enthalpically favourable formation of hydrogen bonds, salt links, and van der Waals interactions with the protein. However, there is another contributor to the enthalpic term and that is the sulphonate group of GSO_3^-, for which a similar argument can be applied as for the sulphonate group of ANS, i.e., unfavourable enthalpic contribution due to desolvation of the sulphonate group upon burial at the H-site and favourable enthalpic contribution due to the formation of a hydrogen bond with the Arg15 guanidino group. Arg15 is a conserved residue in the alpha class GSTs, and it provides electrostatic stabilisation of the thiolate anion of glutathione in conjunction with the Tyr9 (Bjornestedt *et al.*, 1995). The substitution of Arg15 with Leu would eliminate the electrostatic contribution coming from the Arg15 and would place more emphasis on the hydrophobic interactions as the methylene groups are still retained via the substitution. The resultant lack of ion-pair formation, (unless the same is compensated to some extent by Tyr9 proximity and/or placement of water molecule(s)) would result in decrease of the exothermic contribution from the Arg15-ANS/ GSO_3^- sulphonate group ion-pair.

A favourable contributor to the enthalpic terms of both R15L·ANS and R15L·GSO_3^- complex formation is the localisation of the protein C-terminal region. However, the

extent of the contribution will be determined by the initial structural state of the region, as well as proximity to the protein's surface and bound ligand. In a recent crystallographic and calorimetric study done with I219A variant (Kuhnert *et al.*, 2005), it was proposed that the entropic contribution of the coil-to-helix folding of helix 9 in the C-terminal region would be about -44kJ/mol. However, the observed enthalpy for the binding of *S*-hexyl glutathione to hGST A1-1 was -61kJ/mol at 25°C, resulting in 17kJ/mol to account for the non-covalent bonds formed between the inhibitor and the protein and between the folded C-terminal region and the protein. Thus, it was concluded that the C-terminal region was not fully disordered, as 17kJ/mol is insufficient to account for the non-covalent bond formation mentioned above (Kuhnert *et al.*, 2005). The enthalpy of both R15L·ANS (-42kJ/mol at 25°C) and R15L·GSO_3^- (-59kJ/mol at 25°C) complex formation is consistent with the conclusion reached upon the conformation of the C-terminal region.

Although theoretically there is no precedence for the inaccuracies in the value of enthalpy at low c-values, the experimental evidence is inconclusive (Turnbull and Daranas, 2003). The values of the computed enthalpy at 25°C for the 18-crown-6 model· KCl complex formation increased by 12 % with increasing 18-crown-6 concentration, hence increasing c-values (0.01-10). The inaccuracies in the value of enthalpy (Turnbull and Daranas, 2003) has been suggested to be a result of either deviation from unity of the activity of the titrated solution as the concentration of protein and ligand at these low c-value conditions are quite high, or the inaccuracies are result of improper fitting of the thermogram. Therefore, it would be difficult to ascertain the amount of error introduced upon the computation of the enthalpy for the R15L·ANS complex formation.

Inaccuracy of the enthalpy term will result in inaccuracy in the entropic term due to the way the entropic term is calculated. As the ΔG is known via the assessment of the K_a value and the enthalpy term is directly measured, the $T\Delta S$ term is evaluated via the Gibbs-Helmholtz equation (equation (6)).

As reflected above, the entropic contributors to the free energy of complexation are the changes in conformational degrees of freedom (ΔS_{conf}) and changes in solvation (ΔS_{solv}).

The entropic term, $T\Delta S_{obs}$, for the binding of ANS by R15L over the temperature range investigated (5-25°C) is positive reflecting a favourable entropy change of solvation of the restrained water molecules at the binding interfaces of R15L·ANS complex. The

restricted water molecules would solvate the non-polar/polar residues found at the water accessible parts of the H-site and the C-terminal region, the non-polar surfaces of the aromatic ring systems and the negatively charged sulphonate group of the free ANS (Dirr *et al.*, 2005; Sayed *et al.*, 2002). The conformational entropy loss will have a small reducing effect on the positive $T\Delta S_{obs}$ term, as there is a loss of the degrees of freedom at the interface between R15L and ANS. Free ANS conformation is defined by one dihedral angle and one torsion angle which in itself restricts on the movement of the molecule (Ory and Banaszak, 1999; van Holde, 1998). As these events occur, the enthalpy associated with desolvation contributing unfavourably to the complex formation will be overridden by the favourable enthalpy of binding. For the wt hGST A1-1·ANS complex formation, only at temperatures below 17°C is the entropy contribution favourable (Sayed *et al.*, 2002), indicating that at higher temperatures, the desolvation of the above mentioned surfaces is not sufficient to compensate for the losses in conformational entropy. Such losses come from the association of the ANS and protein groups including the C-terminal region as well. The very same terminal region is localised on the binding of another H-site ligand, ethacrynic acid (Cameron *et al.*, 1995). However, as there is no experimental structure, the situation with ANS is not clear. Given that the putative interactions of ANS in the region are similar to those involved in the binding of ethacrynic acid (Cameron *et al.*, 1995; Dirr *et al.*, 2005), it is plausible that the complex formation of hGST A1-1·ANS induces localisation of the C-terminal region and thus contributing unfavourably to entropy. The very same localisation of the C-terminal region will contribute favourably towards the enthalpy term because of the additional interactions at the interfaces between the region, protein and ANS. However, the positive contribution of the R15L·ANS complex formation entropy suggests that ANS binding to the variant over the investigated temperature range (5 to 25°C) does not induce localisation of the C-terminal region resulting in a less favourable enthalpy.

The negative $T\Delta S_{obs}$ of the R15L·GSO_3^- complex formation over the experimental range reflects a net unfavourable entropy change due to loss of degrees of freedom of the binding interfaces enhanced also by the loss of degrees of freedom of the C-terminal region upon ligand binding. Despite the fact that there are no experimental structures for wt hGST A1-1-GSO_3^- complex, the structure of rGST A1-1·GSO_3^- is shown to induce

localisation of the C-terminal end of the protein (Adman *et al.*, 2001). The unfavourable entropy will be attenuated by the desolvation of the interacting surfaces, namely the G- and H-sites, and the C-terminal region on the protein as well as the ligand GSO_3^-. Free glutathione sulphonate has 13 dihedral angles and 13 torsion angles which does not significantly restrain its conformational degrees of freedom when it is free in solution. However, these degrees of freedom will be lost upon binding due to hydrogen bonds and salt link formation as described above. The positive enthalpy associated with desolvation will attenuate the favourable enthalpy of binding. The negative entropy in the investigated temperature range implies that the desolvation of the interacting surfaces is inadequate to compensate for the losses in the conformational entropy. These losses, as mentioned above, include the interacting protein (including the C-terminal region) and the ligand. Despite the fact that there are no experimental structures for wt hGST A1-1-GSO_3^- , the localisation of the C-terminal region upon binding is strongly supported by the experimental structure of rGST A1-1-GSO_3^- complex (Adman *et al.*, 2001) and also by the nature of binding of glutathione conjugated with ethacrynic acid to hGST A1-1 (Cameron *et al.*, 1995). Further, the localisation of the C-terminal region would contribute favourably to enthalpy due to the additional interactions at the interface between the region, protein and GSO_3^-. However, such C-terminal region localisation will contribute unfavourably to the entropy and such localisation might be the major contributor to the entropic term, which is doubled for the R15L (-36kJ/mol at 25°C) relative to the wild type (-18kJ/mol at 25°C) (Sayed, unpublished results). The doubling of the entropy value of R15L relative to the wild type protein suggests that either less water molecules are expelled from the active site in complex formation or that the complex is more restrained in the degrees of freedom or that the localisation of the C-terminal is also far more restrained or there is a combination of all these factors.

Changes in heat capacity (ΔC_p), when complexation occurs, originate primarily from the change in the hydration of polar and nonpolar surface area, thus allowing prediction of the parameter using structural information (Perozzo *et al.*, 2004; Sturtevant, 1977). The contribution towards the heat capacity term when nonpolar surface area is buried is greater, yielding negative ΔC_p, relative to the burial of polar surface area which has smaller effect, yielding positive ΔC_p (Loladze *et al.*, 2001).

The heat capacity of R15L·ANS complex formation is negative (-0.67kJ.mol^{-1}.K^{-1}), which is consistent in sign. However, it is reduced in value relative to wild type protein (-0.84 kJ.mol^{-1}.K^{-1}) (Sayed *et al.*, 2002), thus indicating that there are significant differences in the amount of solvent-exposed non-polar surface area buried on binding. This could be due to the lack of localisation of the C-terminal region over the investigated temperature range.

The heat capacity of R15L·GSO_3^- complex formation is negative (-0.59kJ.mol^{-1}.K^{-1}) and is not significantly different from the wild type protein (-0.63kJ.mol^{-1}.K^{-1}; Sayed *et al.*, 2002) indicative that there are no significant differences in the type and amount of solvent exposed surface area buried on binding of the ligand to the variant R15L.

The difference between the heat capacity of R15L·ANS and R15L·GSO_3^- complex formation reflects the fact that ANS is accommodated in a more hydrophobic environment than GSO_3^- and that ANS does not induce localisation of the C-terminal α9 helix.

4.3 Conclusion

The generation of R15L variant excludes the contribution of positive charge at the active site of wt hGST A1-1 i.e. exclusion of the guanidino group of Arg15. There are two consequences of the Arg15 guanidino group exclusion; the one is consequence for the interdomain interface and the other for the active site of wt hGST A1-1. The import of Arg15 at the interdomain interface is reflected by the fact that the two-state unfolding pathway is changed for the R15L variant. It is possible that the local packing around the substitution region (Figure 4 (B)) has changed. This conclusion is supported by the lack displacement of ANS by GSO_3^- where both ligands are proposed to be accommodated simultaneously in the active site of R15L variant, but not in the active site of wt hGST A1-1. The placement of ANS is argued to be at the H-site whereas GSO_3^- occupies the G-site of hGST A1-1. The binding of ANS is both enthalpically and entropically favourable over the temperature range investigated (5 to 25°C). Thus, indicating expulsion of water molecules from the active site as well as the lack of a localised C-terminal α9 helix. The hydrophobic character of both the ligand and the site which accommodates it (H-site) contribute favourably towards the reaction enthalpy. ANS is conformationaly more

constrained than GSO_3^- when found free in solution, thus exhibiting more favourable conformational entropy change upon binding to R15L variant. The binding of GSO_3^- is enthalpically favourable but entropically opposed. The expulsion of water molecules from the G-site, which accommodates GSO_3^-, is insufficient to compensate for the loss of conformational entropy of both the ligand and C-terminal α9 helix, which becomes localised upon binding. However, favourable enthalpic contributions arise from the formation of hydrogen bonds, salt links and van der Waals contacts between the R15L variant and the ligand and the C-terminal α9 helix.

Chapter 5

References:

Adman, E. T., Le Trong, I., Stenkamp, R. E., Nieslanik, B. S., Dietze, E. C., Tai, G., Ibarra, C. and Atkins, W. M. (2001) Localization of the C-terminus of rat glutathione S-transferase A1-1: crystal structure of mutants W21F and W21F/F220Y. *Proteins* **42**, 192-200.

Allardyce, C. S., McDonagh, P. D., Lian, L. Y., Wolf, C. R. and Roberts, G. C. (1999) The role of tyrosine-9 and the C-terminal helix in the catalytic mechanism of Alpha-class glutathione S-transferases. *Biochem. J.* **343**, 525-31.

Baker, B. M. and Murphy, K. P. (1996) Evaluation of linked protonation effects in protein binding reactions using isothermal titration calorimetry. *Biophys. J.* **71**, 2049-55.

Bjornestedt, R., Stenberg, G., Widersten, M., Board, P. G., Sinning, I., Jones, T. A. and Mannervik, B. (1995) Functional significance of arginine 15 in the active site of human class alpha glutathione transferase A1-1. *J. Mol. Biol.* **247**, 765-73.

Board, P. G., Baker, R. T., Chelvanayagam, G. and Jermiin, L. S. (1997) Zeta, a novel calss of glutathione transferases in a range of species from plants to humans. *Biochem. J.* **328**, 929-935

Board, P. G., Coggan, M., Chelvanayagam, G., Easteal, S., Jermiin, L. S., Shulte, G. K., Danley, D. E., Hoth, L. R., Griffor, M. C., Kamath, A. V., Rosner, M. H., Chrunyk, B. A., Perregaux, D. E., Gabel, C. A., Geoghegan, K. F. and Pandit, J. (2000) Identifiacation, charactrisation and crystal structure of the Omega class glutathione transferases. *J. Biol. Chem.* **275**, 24798-24806

Bowie, J. U. and Sauer, R. T. (1989) Equilibrium dissociation and unfolding of the Arc repressor dimer. *Biochemistry* **28**, 7139-7143

Cameron, A. D., Sinning, I., L'Hermite, G., Olin, B., Board, P. G., Mannervik, B. and Jones, T. A. (1995) Structural analysis of human alpha-class glutathione transferase A1-1 in the apo-form and in complexes with ethacrynic acid and its glutathione conjugate. *Structure* **3**, 717-27.

Chang, L.-H., Fan, J.-Y., Liu, L.-F., Tsai, S.-P. and Tam, M. F. (1992) Cloning and expression of chick liver glutathione S-transferase CL 3 subunit with the use of baculovirus expression system. *Biochem. J.* **281**, 545-551

Dirr, H., Reinemer, P. and Huber, R. (1994) X-ray crystal structure of cytosolic glutathione S-transferases. Implications for protein architecture, substrate recognition and catalytic function. *Eur. J. Biochem.* **220**, 645-661

Dirr, H. W. and Reinemer, P. (1991) Equilibrium unfolding of class pi glutathione S-transferase. *Biochem. Biophys. Res. Commun.* **180**, 294-300.

Dirr, H. W. and Wallace, L. A. (1999) Role of the C-terminal helix 9 in the stability and ligandin function of class alpha glutathione transferase A1-1. *Biochemistry* **38**, 15631-40.

Dirr, H. W., Little, T., Kuhnert, D. C. and Sayed, Y. (2005) A conserved N-capping motif contributes significantly to the stabilization and dynamicsof the C-terminal region of class alpha glutathione transferases. *J. Biol. Chem.* **9**, 9

Doyle, M. L. (1997) Charactrisation of binding interactions by isothermal titration calorimetry. *Curr. Opin. Biotech.* **8**, 31-35

Doyle, M. L., Louie, G., Dal Monte, P. R. and Sokoloski, T. D. (1995) Tight binding affinities determined from thermodynamic linkage to protons by titration calorimetry. *Methods Enzymol.* **259**, 183-94.

Dunitz, J. D. (1995) Win some, lose some: enthalpy-entropy compensation in weak intermolecular interactions. *Chem. Biol.* **2**, 709-12.

Erhardt, J. and Dirr, H. (1995) Native dimer stabilizes the subunit tertiary structure of porcine class pi glutathione S-transferase. *Eur. J. Biochem.* **230**, 614-20.

Erhardt, J. and Dirr, H. (1996) Effect of glutathione, glutathione sulphonate and S-hexylglutathione on the conformational stability of calss pi glutathione S-transferase. *FEBS Lett.* **391**, 313-316

Fukada, H. and Takahashi, K. (1980) Calorimetric study of the reduction of the disulfide bonds in insulin. *J. Biochem. (Tokyo)* **87**, 1111-7.

Gohlke, H. and Klebe, G. (2002) Approaches to the Description and Prediction of the Binding affinity of Small-Molecule Ligands to Macromolecular Receptors. *Angew. Chem. Int. Ed.* **41**, 2644-2676

Graminski, G. F., Kubo, Y. and Armstrong, R. N. (1989) Spectroscopic and kinetic evidence for the thiolate anion of glutathione at the active site of glutathione S-transferase. *Biochemistry* **28**, 3562-3568

Guex, N. and Peitsch, M. C. (1997) SWISS-MODEL and Swiss-Pdb Viewer: an environment for comperative protein modelling. *Electrophoresis* **18**, 2714-2723

Habig, W. H. and Jakoby, W. B. (1981) Assay for differntiation of glutathione S-transferases. *Method. Enzymol.* **77**, 398-405

Habig, W. H., Pabst, M. J. and Jakoby, W. B. (1976) Glutathione S-transferase AA from Rat Liver. *Arch Biochem Biophys.* **175**, 710-716

Hayes, J. D. and Pulford, D. J. (1995) The Glutathione S-transferase Supergene Family: Regulation of GST and the contribution of the Isoenzymes to Cancer Chemoprotection and Drug Resistance. *Crit. Rev. Biochem. Mol. Biol.* **30**, 445-600

Holmgren, A., Soderburg, B. O., Eklund, H. and Branden, C. I. (1975) Three-dimentional structure of Escherichia coli thioredoxin-S2 to 2.8 A resolution. *Proc. Natl. Acad. Sci. U S A* **72**, 2305-2309

Hornby, J. A. T., Luo, J. K., Stevens, J. M., Wallace, L. A., Kaplan, W., Armstrong, R. N. and Dirr, H. W. (2000) Equilibrium folding of dimeric class mu glutathione transferases involves a stable monomeric intermediate. *Biochemistry* **39**, 12336-12344

Jakoby, V. M., Miller, K., Toner, J., Bauman, A., Cheng, L., Li, E. and Cistola, D. (1993) Lignand-binding electrostatic intereactions govern the specificity of retinol- and fatty acid binding proteins. *Biochemistry* **32**, 872-878

Jelesarov, I. and Bosshard, H. R. (1999) Isothermal titration calorimetry and differential scanning calorimetry as complementary tools to investigate the energetics of biomolecular recognition. *J. Mol. Recognit.* **12**, 3-18.

Kaplan, W., Husler, P., Klump, H., Erhardt, J., Sluis-Cremer, N. and Dirr, H. (1997) Conformational stability of pGEX-expressed Schistosoma japonicum glutathione S-transferase: a detoxification enzyme and fusion-protein affinity tag. *Protein Sci.* **6**, 399-406.

Khalifah, R. G., Zhang, F., Parr, J. S. and Rowe, E. S. (1993) Thermodynamics of binding of the CO2-competitive inhibitor imidazole and related compounds to human carbonic anhydrase I: an isothermal titration calorimetry approach to studying weak binding by displacement with strong inhibitors. *Biochemistry* **32**, 3058-66.

Kirk, W. R., Kurian, E. and Prendergast, F. G. (1996) Characterisation of the Sources of Protein-Ligand Affinity: 1-Sulfonato-8-(1')anilinonaphtalene binding to Intestinal Fatty Acid Binding Protein. *Biophys. J.* **70**, 69-83

Kolobe, D., Sayed, Y. and Dirr, H. W. (2004) Characterization of bromosulphophthalein binding to human glutathione S-transferase A1-1: thermodynamics and inhibition kinetics. *Biochem. J.* **382**, 703-9.

Kuhnert, D. C., Sayed, Y., Mosebi, S., Sayed, M., Sewell, T. and Dirr, H. W. (2005) Tertiary Interactions Stabilise the C-terminal Region of Human Glutathione transferase A1-1: a crystalographyc and Calorinmetric Study. *J. Mol. Biol.* **349**, 825-838

Laemmli, U. K. (1970) Cleavage of structural proteins during assembly of the head of bacteriophage T4. *Nature* **227**, 680-685

Lartigue, A., Gruez, A., Spinelli, S., Riviere, S., Brossut, R., Tegoni, M. and Cambillau, C. (2003) The crystal structure of a cockroach pheromone-binding protein suggests a new ligand binding and release mechanism. *J. Biol. Chem.* **278**, 30213-8. Epub 2003 May 23.

Le Trong, I., Stenkamp, R. E., Ibarra, C., Atkins, W. M. and Adman, E. T. (2002) 1.3-A resolution structure of human glutathione S-transferase with S-hexyl glutathione bound reveals possible extended ligandin binding site. *Proteins* **48**, 618-27.

Leavitt, S. and Freire, E. (2001) Direct measurement of protein binding energetics by isothermal titration calorimetry. *Curr. Opin. Struct. Biol.* **11**, 560-6.

Loladze, V. V., Ermolenko, D. N. and Makhatadze, G. I. (2001) Heat capacity changes upon burial of polar and nonpolar groups in proteins. *Protein Sci.* **10**, 1343-1352

Lumry, R. and Rajender, S. (1970) Enthalpy-entropy compensation phenomena in water solutions of proteins and small molecules: a ubiquitous property of water. *Biopolymers* **9**, 1125-227.

Lyon, R. P. and Atkins, W. M. (2002) Kinetic characterization of native and cysteine 112-modified glutathione S-transferase A1-1: reassessment of nonsubstrate ligand binding. *Biochemistry* **41**, 10920-7.

Makhatadze, G. I. and Privalov, P. L. (1990) Heat capacity of proteins. I. Partial molar heat capacity of individual amino acid residues in aqueous solution: hydration effect. *J. Mol. Biol.* **213**, 375-84.

Makhatadze, G. I. and Privalov, P. L. (1996) On entropy of protein folding. *Protein Sci.* **5**, 507-510

Mannervik, B., Alin, P., Guthenburg, C., Jensson, H., Tahir, M. K., Warholm, M. and Jornvall, H. (1985) Identifiaction of three classes of cytosolic glutathione transferase common to several mammalian species: correlation between structural data and enzymatic properties. *Proc. Natl. Acad. Sci. U S A* **82**, 7202-7206

Matulis, D. and Lovrien, R. (1998) 1-Anilino-8-naphthalene sulfonate anion-protein binding depends primarily on ion pair formation. *Biophys. J.* **74**, 422-9.

McGavin, D., *Thermodynaimics and Statistical Thermodynamics*, in *Biophysics Textbook Online*. 2004.

McMurry, J., *Organic chemistry*. 4th ed. 1996: Brooks/Cole Publishing Company. 597-599.

Meyer, D. J., Coles, B., Pemble, S. E., Gilmore, K. S., Fraser, G. M. and Ketterer, B. (1991) Theta, a new calss of glutathione transferase purified from rat and man. *Biochem. J.* **274**, 409-414

Mosebi, S., Sayed, Y., Burke, J. and Dirr, H. W. (2003) Residue 219 impacts on the dynamics of the C-terminal region in glutathione transferase A1-1: implications for stability and catalytic and ligandin functions. *Biochemistry* **42**, 15326-32.

Ory, J. J. and Banaszak, L. J. (1999) Studies of the ligand binding reaction of adipocyte lipid binding protein using the fluorescent probe 1, 8-anilinonaphthalene-8-sulfonate. *Biophys. J.* **77**, 1107-16.

Pace, C. N. (1986) Determination and analysis of urea and guanidine hydrochloride denaturation curves. *Methods Enzymol.* **131**, 266-80.

Pace, C. N., Shirley, B. A. and Thomson, J. A., *Measuring conformational stability of a protein*, in *Protein structure: A Practical Approach*, T. E. Creighton, Editor. 1989, IRL Press, Oxford University Press: Oxford. p. 311-330.

Papworth, C., Bauer, J. C., Braman, J. and Wright, D. A. (1996) Site-directed mutagenesis using double-stranded plasmid DNA templates. *Strategies* **9**, 3-4

Pemble, S. E., Wardle, A. F. and Taylor, J. B. (1996) Glutathione S-transferase class Kappa: characterization by the cloning of rat mitochondrial GST and identifiacation of human homologue. *Biochem. J.* **319**, 749-754

Perkins, S. J. (1986) Protein volumes and hydration effects. *Eur. J. Biochem.* **319**, 749-754

Perozzo, R., Folkers, G. and Scapozza, L. (2004) Thermodynamics of Protein-Ligand Interactions: History, Presence, and Future aspects. *J Recept Signal Transduct Res.* **24**, 1-52

Pierce, M. M., Raman, C. S. and Nall, B. T. (1999) Isothermal Titration Calorimetry of Protein-Protein Interactions. *Methods* **19**, 213-221

Privalov, P. L., in *Protein Folding*, T. Creighton, Editor. 1992, W. H. Freeman & Co.: New York. p. 88-91.

Sayed, Y., Hornby, J. A., Lopez, M. and Dirr, H. (2002) Thermodynamics of the ligandin function of human class Alpha glutathione transferase A1-1: energetics of organic anion ligand binding. *Biochem. J.* **363**, 341-6.

Schmid, F. X., in *Protein Folding*, T. Creighton, Editor. 1992, W. H. Freeman & Co.: New York. p. 199-203.

Schonbrunn, E., Eschenburg, S., Luger, K., Kabsch, W. and Amrhein, N. (2000) Structural basis for the interaction of the fluorescence probe 8-anilino-1-naphthalene sulfonate (ANS) with the antibiotic target MurA. *Proc. Natl. Acad. Sci. U S A* **97**, 6345-9.

Sigurskjold, B. W. (2000) Exact analysis of competition ligand binding by displacement isothermal titration calorimetry. *Anal. Biochem.* **277**, 260-6.

Sinning, I., Kleywegt, G. J., Cowan, S. W., Reinemer, P., Dirr, H. W., Huber, R., Gilliland, G. L., Armstrong, R. N., Ji, X., Board, P. G. and et al. (1993) Structure determination and refinement of human alpha class glutathione transferase A1-1, and a comparison with the Mu and Pi class enzymes. *J. Mol. Biol.* **232**, 192-212.

Stenberg, G., Board, P. G. and Mannervik, B. (1991b) Mutation of an evolutionary conserved tyrosine residue in the active site of human class Alpha glutathione transferase. *FEBS Lett.* **293**, 153-155

Stenberg, G., Bjornestedt, R. and Mannervik, B. (1992) Heterologous expression of recombinant human glutathione transferase A1-1 from a hepatoma cell line. *Protein. Expr. Purif.* **3**, 80-4.

Stenberg, G., Board, P. G., Carlsberg, I. and Mannervik, B. (1991a) Effects of directed mutagenesis on conserved arginine residues in human Class Alpha glutathione transferese. *Biochem. J.* **274**, 549-555

Stevens, J. M., Hornby, J. A., Armstrong, R. N. and Dirr, H. W. (1998) Class sigma glutathione transferase unfolds via a dimeric and a monomeric intermediate: impact of subunit interface on conformational stability in the superfamily. *Biochemistry* **37**, 15534-15541

Sturtevant, J. M. (1977) Heat capacity and entropy changes in processes involving proteins. *Proc. Natl. Acad. Sci. U S A* **74**, 2236-2240

Turnbull, W. B. and Daranas, A. H. (2003) On the value of c: can low affinity systems be studied by isothermal titration calorimetry? *J. Am. Chem. Soc.* **125**, 14859-66.

van Holde, K. E., Johnson, C., Ho, P.S., *Principles of Physical Biochemistry*. 1998, New Jersey: Prentice-Hall, Inc.

Wallace, A. C., Laskowski, R. A. and Thornton, J. M. (1995) LIGPLOT: aprogram to generate schematic diagrams of protein-ligand interactions. *Protein Eng.* **8**, 127-134

Wallace, L., Blatch, G. L. and Dirr, H. W. (1998a) A topologically conserved aliphatic residue in alpha-helix 6 stabilises the hydrophobic core in domain II of glutathione

transferases and is a structural determinant for the unfolding pathway. *Biochem. J.* **336**, 413-418

Wallace, L., Burke, J. and Dirr, H. W. (2000) Domain-domain interface packing at conserved Trp-20 in class α glutathione transferse impacts on protein stability. *Biochem. Biophys. Acta* **1478**, 325-332

Wallace, L. A., Sluis-Cremer, N. and Dirr, H. W. (1998b) Equilibrium and kinetic unfolding properties of dimeric human glutathione transferase A1-1. *Biochemistry* **37**, 5320-8.

Widersten, M., Bjornestedt, R. and Mannervik, B. (1996) Involvement of the carboxyl groups of glutathione in the catalytic mechanism of human glutathione transferese A1-1. *Biochemistry* **35**, 7731-7742

Wiesner, S., Kurian, E., Prendergast, F. G. and Halle, B. (1999) Water Molecules in the Binding Cavity of Intestinal Fatty Acid Binding Protein: Dynamic Characterisation by Water ^{17}O and ^{2}H Magnetic Relaxation Dispersion. *J. Mol. Biol.* **286**, 233-246

Wilce, M. C. J. and Parker, M. W. (1994) Structure and function of glutathione S-transferses. *Biochim. Biophys. Acta* **1205**, 1-18

Winder, A. F. and Gent, W. L. (1971) Correction of light-scattering errors in spectrophotometric protein determinations. *Biopolymers* **10**, 1243-1251

Wiseman, T., Williston, S., Brandts, J. F. and Lin, L. N. (1989) Rapid measurement of binding constants and heats of binding using a new titration calorimeter. *Anal. Biochem.* **179**, 131-7.